A NEW PROPOSED METHOD OF CONTINGENCY RANKING

A Thesis
Presented to
The Academic Faculty

by

Stephanie Mizzell Gossman

In Partial Fulfillment
of the Requirements for the Degree
Master of Science in the
School of Electrical and Computer Engineering

Georgia Institute of Technology
August 2010

A NEW PROPOSED METHOD OF CONTINGENCY RANKING

Approved by:

Dr. A. P. Meliopoulos, Advisor
School of Electrical and Computer Engineering
Georgia Institute of Technology

Dr. Ronald Harley
School of Electrical and Computer Engineering
Georgia Institute of Technology

Dr. C. Santiago Grijalva
School of Electrical and Computer Engineering
Georgia Institute of Technology

Date Approved: May 14, 2010

I dedicate this thesis to several influential men in my life. First, my husband (Kyle Gossman), who has been wonderfully supportive; second, my father (George Mizzell, Jr.) who has encouraged me from an early age to pursue my goals; and third, my grandfathers (George Mizzell, Sr. and George O'Kelley) who were always so proud of my achievements and would love to read about my work if they could.

ACKNOWLEDGEMENTS

This research has been funded by Georgia Power Company through Dr. A. P. Meliopoulos' Georgia Power Chair. I am very thankful for the support of Georgia Power in allowing me to pursue this research topic.

I would like to thank my advisor, Dr. A. P. Meliopoulos, for his patience and guidance through my research and time at Georgia Tech. Dr. Meliopoulos has helped explain the theory behind this work and also helped develop the problem and solution approach.

I am also grateful for the MS Thesis reading committee members, Dr. Ronald Harley and Dr. C. Santiago Grijalva, and their willingness to support and help improve this thesis.

A special word of thanks also goes to Dr. George Cokkinides. His matrix sparsity software improved the efficiency of my work by allowing me to take advantage of the sparsity that exists in the matrices that describe power systems.

Finally, I would like to thank Kyle Gossman, my husband, for the time he took to help improve my coding and debugging skills. I would not have been able to complete this project as quickly if it were not for his willingness to share his expertise in software development.

TABLE OF CONTENTS

		Page
ACKNOWLEDGEMENTS		iv
LIST OF TABLES		vii
LIST OF FIGURES		viii
LIST OF SYMBOLS		x
LIST OF ACRONYMS AND INITIALISMS		xv
SUMMARY		xvi
CHAPTER		
1	INTRODUCTION	1
2	LITERATURE REVIEW	4
	2.1 Introduction	4
	2.2 Proposed Research Definition	6
	2.3 Future Modifications and Improvements	12
	2.4 Chapter Summary	16
3	CONTINGENCY ANALYSIS OVERVIEW	17
	3.1 The Contingency Analysis Process	17
	3.2 Chapter Summary	21
4	QUADRATIZED POWER FLOW MODEL OVERVIEW	22
	4.1 The Quadratized Power Flow Model for Circuit Elements	22
	4.2 Chapter Summary	27
5	INPUT FILE FORMAT	29
	5.1 PTI Data Format	29
	5.2 Chapter Summary	33
6	PROBLEM DEFINITION AND FORMULATION	34
	6.1 Performance Index Definition	34

6.2 Solving for the State of the System 37
6.3 Solving for the Costate Vector 45
6.4 Calculation of ΔJ for Contingencies 50
6.5 Chapter Summary 53
7 TEST SYSTEM AND RESULTS 55
7.1 Test System 55
7.2 Chapter Summary 73
8 CONCLUSIONS, CONTRIBUTIONS, and RECOMMENDATIONS 76
8.1 Comparing Results 76
8.2 Contributions 78
8.3 Recommendations for Future Research 79
APPENDIX A: SPARSITY TECHNIQUES 84
A.1 LU Factorization 84
APPENDIX B: ADDITIONAL DATA 87
B.1 Introduction 87
B.2 Test System and Results 88
REFERENCES 97

LIST OF TABLES

Page

Table 7.1. Test System Line Ratings [10]. 57

Table 8.1. Linear Approximation Error for $J_{1,1}$. 77

Table 8.2. Linear Approximation Error for $J_{1,2}$. 77

Table 8.3. Linear Approximation Error for J_2. 77

Table 8.4. Comparison of Average Errors for $J_{1,1}$, $J_{1,2}$, and J_2. 78

Table 8.5. Linear Approximation Errors for J_3. 83

Table B.1. Total Energy Consumed in United States in 1980-2006 [1]. 87

Table B.2. PTI Format for Test System Input Data. 89

Table B.3. Results from Circuit 1-5 Outages for $J_{1,1}$. 90

Table B.4. Results from Circuit 1-5 Outages for $J_{1,2}$. 91

Table B.5. Results from Circuit 1 Outage for J_2. 91

Table B.6. Results from Circuit 2 Outage for J_2. 92

Table B.7. Results from Circuit 3 Outage for J_2. 92

Table B.8. Results from Circuit 4 Outage for J_2. 93

Table B.9. Results from Circuit 5 Outage for J_2. 93

Table B.10. Results from Circuit 1 Outage for J_3. 94

Table B.11. Results from Circuit 2 Outage for J_3. 94

Table B.12. Results from Circuit 3 Outage for J_3. 95

Table B.13. Results from Circuit 4 Outage for J_3. 95

Table B.14. Results from Circuit 5 Outage for J_3. 96

LIST OF FIGURES

Page

Figure 1.1. Energy consumption of the United States between 1980 and 2006. 1

Figure 2.1. Example test system [10]. 8

Figure 2.2. Nonlinear performance index ($\propto$=1) for given circuit. 9

Figure 2.3. Nonlinear performance index ($\propto$=2) for given circuit. 9

Figure 2.4. More linear performance index for the circuit's transmission overloads. 12

Figure 2.5. More linear performance index for the circuit's transmission margins. 12

Figure 2.6. More linear performance index for the given circuit. 13

Figure 3.1. Pi-equivalent model of a transmission line with control variables [10]. 18

Figure 3.2 Block diagram of the process to calculate ΔJ. 19

Figure 4.1. Circuit line pi-equivalent model [10]. 24

Figure 4.2. Generator equivalent circuit [10]. 25

Figure 4.3. Constant Power Load equivalent circuit components [10]. 27

Figure 6.1. Combination of QPF Model's currents at Bus k. 42

Figure 7.1. Four bus test system [10]. 56

Figure 7.2. Results from circuit 1 outage for $J_{1,1}$. 58

Figure 7.3. Results from circuit 2 outage for $J_{1,1}$. 59

Figure 7.4. Results from circuit 3 outage for $J_{1,1}$. 60

Figure 7.5. Results from circuit 4 outage for $J_{1,1}$. 61

Figure 7.6. Results from circuit 5 outage for $J_{1,1}$. 62

Figure 7.7. Results from circuit 1 outage for $J_{1,2}$. 63

Figure 7.8. Results from circuit 2 outage for $J_{1,2}$. 64

Figure 7.9. Results from circuit 3 outage for $J_{1,2}$. 65

Figure 7.10. Results from circuit 4 outage for $J_{1,2}$. 66

Figure 7.11. Results from circuit 5 outage for $J_{1,2}$. 67

LIST OF FIGURES (2)

Figure 7.12. Results from circuit 1 outage for J_2. 69

Figure 7.13. Results from circuit 2 outage for J_2. 70

Figure 7.14. Results from circuit 3 outage for J_2. 71

Figure 7.15. Results from circuit 4 outage for J_2. 72

Figure 7.16. Results from circuit 5 outage for J_2. 73

Figure 8.1. Results from circuit 1 outage for J_3. 81

Figure 8.2. Results from circuit 2 outage for J_3. 81

Figure 8.3. Results from circuit 3 outage for J_3. 82

Figure 8.4. Results from circuit 4 outage for J_3. 82

Figure 8.5. Results from circuit 5 outage for J_3. 83

LIST OF SYMBOLS

$\propto$	Variable power term for nonlinear performance index
β	Number of branches in a power system
$\in$	A very small scalar number
κ	A specific row number in a matrix or vector
$\boldsymbol{\chi}$	Column vector
$\boldsymbol{A}$	Square, nonsingular, sparse matrix
B	Transmission line pi-equivalent shunt terms (PTI format) [p.u.]
BL	Shunt susceptance for bus load (PTI format) [p.u.]
B_{km}	One-half of shunt terms of pi-equivalent transmission line [p.u.]
$b_{dn,k}$	Nominal susceptance of constant power bus load at bus k [p.u.]
b_{gk}	Susceptance of generator at bus k [p.u.]
b_{km}	Transmission line susceptance between buses k and m [p.u.]
b_{skm}	Shunt susceptance between buses k and m, close to bus k [p.u.]
b_{smk}	Shunt susceptance between buses k and m, close to bus m [p.u.]
CKT	Circuit identifier for a transmission line (PTI format)
c	All possible contingencies
d	Number of constant power loads in a power system
$\tilde{E}_k$	Generator voltage at bus k [p.u.]
$E_{k,imag}$	Imaginary part of generator voltage at bus k [p.u.]
$E_{k,real}$	Real part of generator voltage at bus k [p.u.]
f	Performance index
f_u	Derivative of performance index with respect to contingencies
$f_{u_c}(\boldsymbol{x_{PI}})$	Derivative of augmented performance index with respect to contingency u_c

LIST OF SYMBOLS (2)

$\boldsymbol{f_x}$	Derivative of performance index with respect to state variables
G_k	Second additional generator equation for kth generator
GL	Shunt conductance for bus load (PTI format) [p.u.]
g	Number of generators in a power system
$\boldsymbol{g(x)}$	State power flow equations
$g_{dn,k}$	Nominal conductance of constant power bus load at bus k [p.u.]
g_{km}	Transmission line conductance between buses k and m [p.u.]
$\boldsymbol{g_{margin}(x)}$	Augmented state equations for the margins performance index
$\boldsymbol{g_{margin,u_c}(x_{PI})}$	Derivative of augmented state equations for margins with respect to contingency u_c
$\boldsymbol{g_{margin,x_{PI}}(x_{PI})}$	Derivative of augmented state equations for margins with respect to state variables
$\boldsymbol{g_{over}(x)}$	Augmented state equations for overloads performance index
$\boldsymbol{g_{over,u_c}(x_{PI})}$	Derivative of augmented state equations for overloads with respect to contingency u_c
$\boldsymbol{g_{over,x_{PI}}(x_{PI})}$	Derivative of augmented state equations for overloads with respect to state variables
$\boldsymbol{g_u(x)}$	Derivative of state equations with respect to contingencies
$\boldsymbol{g_{u_c}(x_{PI})}$	Derivative of augmented state equations with respect to contingency u_c
$\boldsymbol{g_{u_{c(k,m)}}(x_{PI})}$	Derivative of augmented state equations with respect to contingency between Buses k and m
$\boldsymbol{g_x(x)}$	Jacobian matrix
$\boldsymbol{g_{x,k}(x)}$	Row k of Jacobian matrix
$\boldsymbol{g_{x_{PI}}(x_{PI})}$	Augmented Jacobian matrix
I	Bus number (PTI format)
ID	Generator machine identifier (PTI format)
IDE	Bus type (PTI format)

LIST OF SYMBOLS (3)

$IREG$	Operation mode of generator (PTI format)
$\tilde{I}_{dk}$	Current flowing to constant power load at bus k [p.u.]
$I_{km,0}$	Current rating of transmission line between buses k and m [p.u.]
$\tilde{I}_{km}$	Current between buses k and m, flowing out of bus k [p.u.]
$I_{km,imag}$	Imaginary component of the complex current from Bus k to Bus m
$I_{km,real}$	Real component of the complex current from Bus k to Bus m
$\tilde{I}_{mk}$	Current between buses k and m, flowing out of bus m [p.u.]
I_{imag}	Imaginary part of transmission line current [p.u.]
I_{real}	Real part of transmission line current [p.u.]
J	Performance index
$J_{1,1}$	First performance index from type 1 definition
$J_{1,2}$	Second performance index from type 1 definition
J_2	Performance index number 2
J_3	Performance index number 3
$\boldsymbol{J_x}$	Derivative of performance index with respect to state variables
J_u	Derivative of performance index with respect to contingencies
k	From Bus
L	Lower triangular matrix
$MBASE$	Total power base of generator (PTI format) [MVA]
m	To Bus
n	Number of buses in the power system
PL	Real power of constant power bus load (PTI format) [MW]
P_{dk}	Real power consumed by constant power load at bus k [p.u.]

LIST OF SYMBOLS (4)

$P_{k,specified}$	Real power at bus k load, as specified by input file [p.u.]
QL	Reactive power of constant power bus load (PTI format) [MVAr]
Q_{dk}	Reactive power consumed by constant power load at bus k [p.u.]
$Q_{k,specified}$	Reactive power at bus k load, as specified by input file [p.u.]
R	Resistance along a transmission line (PTI format) [p.u.]
$RATEA$	Rating of transmission line (PTI format) [MVA]
$SBASE$	Three-phase power base of the power system [MVA]
ST	Status of transmission line (PTI format)
$STAT$	Status of generator (PTI format)
U	Upper triangular matrix
u_{1k}	Constant power load constraint variable 1 at bus k
u_{2k}	Constant power load constraint variable 2 at bus k
u_c	Contingency Control Variable
$u_{c(k,m)}$	The control variable between Bus k and Bus m
VA	Bus voltage angle (PTI format) [deg]
VM	Bus voltage magnitude (PTI format) [p.u.]
VS	Generator's bus voltage set point (PTI format) [p.u.]
$\tilde{V}_k$	Bus voltage at bus k [p.u.]
$V_{k,imag}$	Imaginary part of the bus voltage at bus k [p.u.]
$V_{k,real}$	Real part of the bus voltage at bus k [p.u.]
$V_{k,specified}$	Desired bus voltage for PV generator [p.u]
$\tilde{V}_m$	Bus voltage at bus m [p.u.]
$V_{m,imag}$	Imaginary part of the bus voltage at bus m [p.u.]

LIST OF SYMBOLS (5)

$V_{m,real}$	Real part of the bus voltage at bus m [p.u.]
X	Reactance along a transmission line (PTI format) [p.u.]
$\boldsymbol{x}$	Vector of state variables
$\widehat{\boldsymbol{x}}^{\boldsymbol{T}}$	Costate vector
$\boldsymbol{x_{PI}}$	Augmented state variables vector for proposed performance index
Y_{km}	Transmission line admittance between buses k and m [p.u.]
$Y_{dn,k}$	Nominal admittance of constant power bus load [p.u.]
$\boldsymbol{y}$	Variable column vector
$y_{km,over}$	Variable used to define transmission overload performance index
$y_{km,under}$	Variable used to define transmission margin performance index
y_{skm}	Shunt term admittance between buses k and m, near bus k [p.u.]
y_{smk}	Shunt term admittance between buses k and m, near bus m [p.u.]
ZR	Generator internal resistance (PTI format) [p.u.]
ZX	Generator internal reactance (PTI format) [p.u.]
Z_{km}	Transmission line impedance between buses k and m [p.u.]
$z_{km,a}$	Variable ‘a’ used to impose performance index definition
$z_{km,b}$	Variable ‘b’ used to impose performance index definition

LIST OF ACRONYMS AND INITIALISMS

CDF	Common Data Format
CSV	Comma-Separated Values
IEEE	Institute of Electrical and Electronics Engineers
KCL	Kirchoff's Current Law
LU	Matrix Factorization into Lower- and Upper-Triangular Matrices
NERC	North American Electric Reliability Corporation
NPCC	Northeast Power Coordinating Council
PI	Performance Index
PTI	Power Technologies Incorporated
QPF	Quadratized Power Flow

SUMMARY

Security analysis of a power system requires a process called contingency analysis that analyzes results from all possible single contingencies (i.e. outages) in the system. The process of contingency analysis requires the definition of a parameter that is used to monitor a certain aspect of the system, which is called a performance index. The performance index definitions used traditionally have been highly nonlinear, and the results have not accurately predicted the outcome of the performance index in some cases. These incorrect results are referred to as misrankings since the contingency results are usually placed in order of severity so that the most severe cases are evident.

This thesis considers a new definition of contingency ranking using a more linearized definition of the performance index. The construction of both the new, proposed definition and the classic definition both consider the current loading of circuits in the system as compared to their rated values. Specifically, the parameter measured by the proposed definition measures the difference, while the more nonlinear definition uses a ratio of the two quantities, which is then raised to a higher power.

A small, four bus test system is used to demonstrate the benefits of the new, more linearized definition. The average percent error for all single line contingencies of the system decreased by over 9.5% using the proposed definition as compared to the previous one. This decrease in error allows this performance index to monitor a similar parameter (comparing current loading and current rating of the lines) and achieve a higher degree of accuracy. Further linearization of this proposed definition also shows a reduction in the average percent error by an additional 22% so that when compared to the original, highly nonlinear definition, the average error is reduced by almost 30%. By linearizing the definition of the performance index, the results are more accurate and misrankings are less likely to occur from the security analysis process.

CHAPTER 1

INTRODUCTION

The power industry has seen a significant increase in the demand for electricity in recent years. This increase requires the power providers and the operators who manage their systems to adjust to meet the need while still maintaining safe operating systems. The United States already consumes more total electricity than any other country in the world, and the demand continues to rise. According to data provided by the United States Energy Information Administration, the total energy consumption of the United States has increased by approximately 700 billion kWh every 10 years since 1980, as shown in Figure 1.1 [1]. The data for this figure is given in Table B.1.

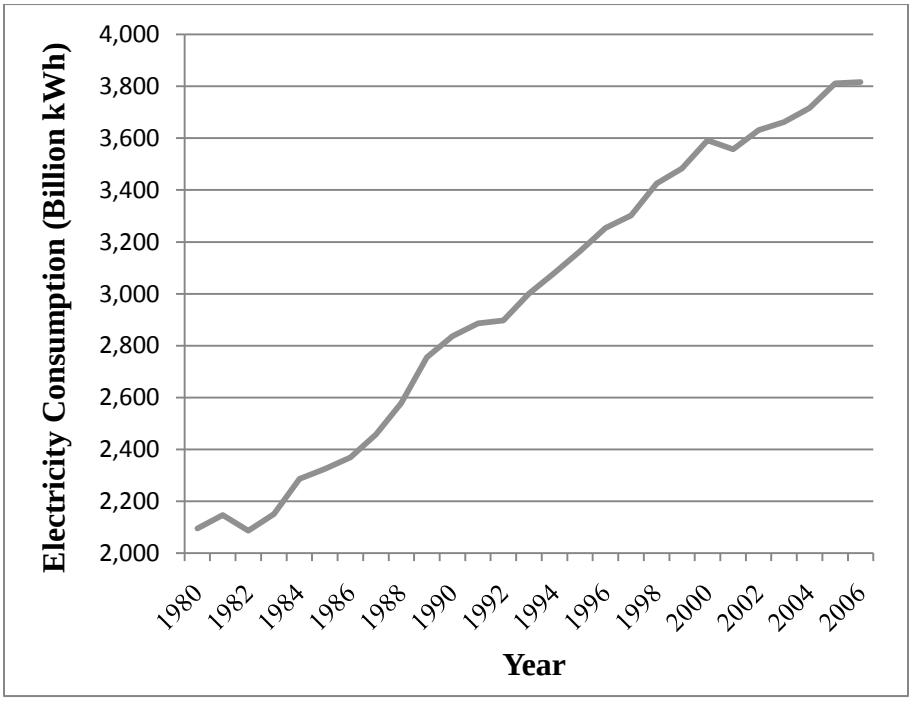

Figure 1.1. Energy consumption of the United States between 1980 and 2006.

One way the systems' operators are able to meet the increasing demand is to operate the systems close to their maximum capacity at peak demand times (e.g. in the summer). Operating a system in this manner gives rise to many potential problems, however, that could be devastating to the system and power providers. Therefore there are security issues and protocols put in place that attempt to ensure the stability and security of the system at all times.

In order to determine standards necessary to properly maintain power systems nationwide, the United States government formed the North American Electric Reliability Corporation (NERC) to act as a regulating agency for the country's electric utility industry. Some of NERC's main focuses include maintaining the reliability and security of the power systems it regulates. The current security standard enforced by NERC and used nationwide requires transmission power systems to operate such that the system could remain secure and stable if one element is suddenly and unexpectedly lost (i.e. outaged). This operation criterion is referred to as "N-1 Contingency" operation, where a contingency is an element that could be lost (e.g. a transmission line) [2]. The risk factor of failing to comply with a minimum of N-1 contingency analysis is considered to be "Medium" on a three point scale ("Low," "Medium," and "High"), which can carry significant consequences [2]. Being "N-1 Contingency" compliant along with other regulations imposed and enforced by NERC set standards to which all operating power systems within the United States must adhere.

This thesis explores the method by which the "N-1 Contingency" operation is determined and proposes a new definition. First, several publications that are related to this topic are examined (Chapter 2), and several suggested future applications and improvements are mentioned from these papers. Then a brief overview of three

necessary topics and concepts are given: the process of Contingency Analysis (Chapter 3), the Quadratized Power Flow (QPF) Model used in the proposed definition (Chapter 4), and sparsity techniques (Appendix A). All of these topics play into the final proposed definition of N-1 Contingency Analysis (Chapter 6). Then a test system is used, and the results from this system are given to compare the proposed method with methods that are currently used (Chapter 7). Conclusions based upon the test results are then presented in Chapter 8.

CHAPTER 2

LITERATURE REVIEW

2.1 Introduction

To be in compliance with NERC's standards, the transmission operators must be able to test for all single contingency cases to see how each contingency affects the system's operating capacity and reliability. If a single contingency case is found that causes inoperable conditions (e.g. an overloaded local line), then the operators must find the best solution for that case so that most of the system could still operate if the contingency were to occur. To test each contingency one at a time is unrealistic in a real-time environment like transmission systems operations, so there has been a push to automate the process so that only the worst single contingency situations are reported to the operators. The operators can then take the shortened list of the most severe contingencies and determine the best solutions for each case so that the power systems they operate will not violate the standards that are in place.

The process overall is referred to as security analysis, which includes evaluating the state of the system and determining the actions necessary to remedy any inoperable situations caused by possible contingencies. Security analysis includes both the need to rank the contingencies based on a given criterion and also to analyze the results using simulations of the system under given contingency conditions. Contingency ranking (also called contingency selection) occurs first using a criterion, called a performance index (PI), against which each of the contingencies is ranked. Then, after the results are obtained, contingency analysis takes place, which requires testing the list of the most severe contingencies to determine the best course of action needed to maintain the system in each potential instance.

Contingency ranking approaches vary, and currently the methods are grouped into three different categories: direct ranking, ranking by one iteration of screening, and fast screening by bounding the solution area [3]. The methods from the first group are not often used since they tend to mask errors in the results, and the methods from the third category have been developed only recently and are not yet widely used in industry [3]. The methods from the second category are the most widely and commonly used in industry, and there are a variety of implementations of these methods, with one of the main variables being the performance index selected [3].

The problems typically associated with methods of ranking by one iteration of screening include inaccurate rankings of the contingencies (called misrankings) and a heavy computational burden. The misranking problem stems from the performance index used to rank the contingencies. Since most performance indexes are nonlinear, they are not always capable of accurately predicting the correct outcome of the system, which results in misrankings. The heavy computational burden of these methods adds to the length of time it takes for such programs to run, and as such, these methods can be not as useful in a real-time environment if they are not implemented efficiently. The computational burden is great with most systems and methods of performing contingency analysis since the systems are large, but one way to improve efficiency of computation is to switch the solution process used to solve for the state of the system. There have been efforts to increase the accuracy of the contingency ranking results, but these efforts focused on linearizing the state of the system instead of the linearization of the PI definition itself [4]. The Quadratized Power Flow (QPF) method presented in [4] attempts to bring the PI definition to near linear conditions by simplifying the equations to have order no greater than two. This model has the advantages of consisting of systems of only quadratic equations and being able to model the complex behavior of elements of the power system accurately [4].

2.2 Proposed Research Definition

The proposed research focuses on a new method of contingency ranking that creates a more linearized performance index based on the overloading and available margins of transmission lines in a power system. Overloads refer to the amount by which a transmission line is loaded beyond its rated capability, while the margins refer to the available loading capability based on the rating of the line. By considering both the overloading and available margins of the transmission lines, this method accounts for both possibilities (instead of a simple ratio of the loading of a line to its rating), which makes this PI definition more realistic. Also, by bringing the performance index closer to a linear form, it is possible to avoid some of the misrankings that might otherwise occur. This method uses the QPF solution technique to simplify the equations by removing most of the nonlinear terms. It also takes advantage of the sparsity of the system's matrices in the calculations to increase the speed of the application.

The nonlinear performance index definition for single contingency analysis given in (2.1) is a popular choice currently in industry and is frequently referenced in publications (e.g. [4], [6], and [10]). For the given performance index, J, the ratio of the current loading along a line (I_β) and its nominal rating ($I_{\beta,0}$) are raised to the power $2 \propto$ (where $\propto > 0$). This ratio is determined for every circuit branch in the system, where β is the number of circuits. This particular performance index considers the current in the circuits of the system, but the current loading and nominal rating terms could be replaced so that the index considers other elements of the system such as power along each line and voltages at each bus.

$$J = \sum_{\beta} \left(\frac{I_{\beta}}{I_{\beta,0}} \right)^{2\propto} \tag{2.1}$$

Performance index definitions of the form given in (2.1) are by nature nonlinear, and they can become highly nonlinear with increasing values of $\propto$. Contingency ranking seeks to provide a performance index whose partial derivative with respect to the contingencies considered can be calculated quickly and accurately. The partial derivative of the performance index is also interpreted as the slope of the performance index with respect to the outaged element. In order to simulate the effect of an outaged element, a control variable, u_c, represents the status of each element, and it multiplies the admittance of each element such that a u_c value of one means the element is in service, and a u_c value of zero means it is out of service (i.e. outaged).

A simple test system, given in Figure 2.1, is used to give preliminary results and demonstrate the utility of the structure of the proposed performance index definition. The contingency considered in this example is that of the line between Bus 1 and Bus 2. As shown in Figure 2.2, when $\propto = 1$, the performance index (shown in blue) becomes increasingly nonlinear as this line is outaged. The slope estimated pre-contingency (before the outage) is shown in red. This linear approximation gives a fairly good estimate of how the performance index of the system will respond to the given outage. There is approximately 6.9% error, which is calculated using (2.2), but for a linear

$$\%\ Error = \left(\frac{Estimated\ Value - True\ Value}{True\ Value} \right) \cdot 100\% \tag{2.2}$$

approximation of a nonlinear function, it gives a good indication of the response. Figure 2.3 shows the result from the same contingency when $\propto = 2$, where the performance index is also shown in blue, and the linear approximation in red. The error for the larger value of $\propto$, calculated according to (2.2), is also larger (16%), which supports the idea that the error obtained when approximating a nonlinear performance index increases with the increasing degree of nonlinearity of the index itself.

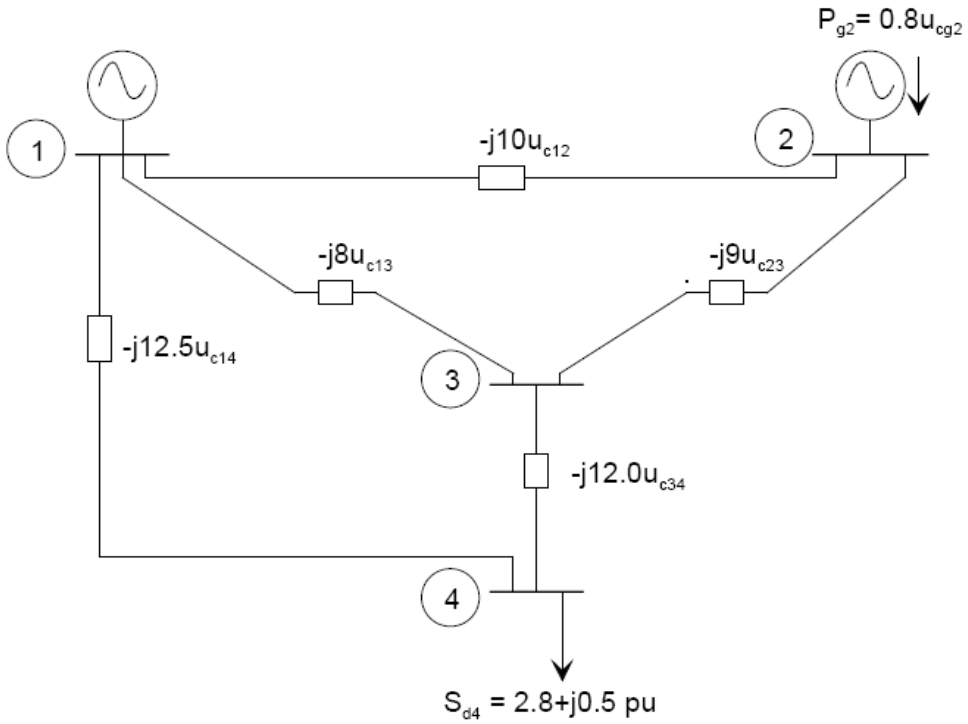

Figure 2.1. Example test system [10].

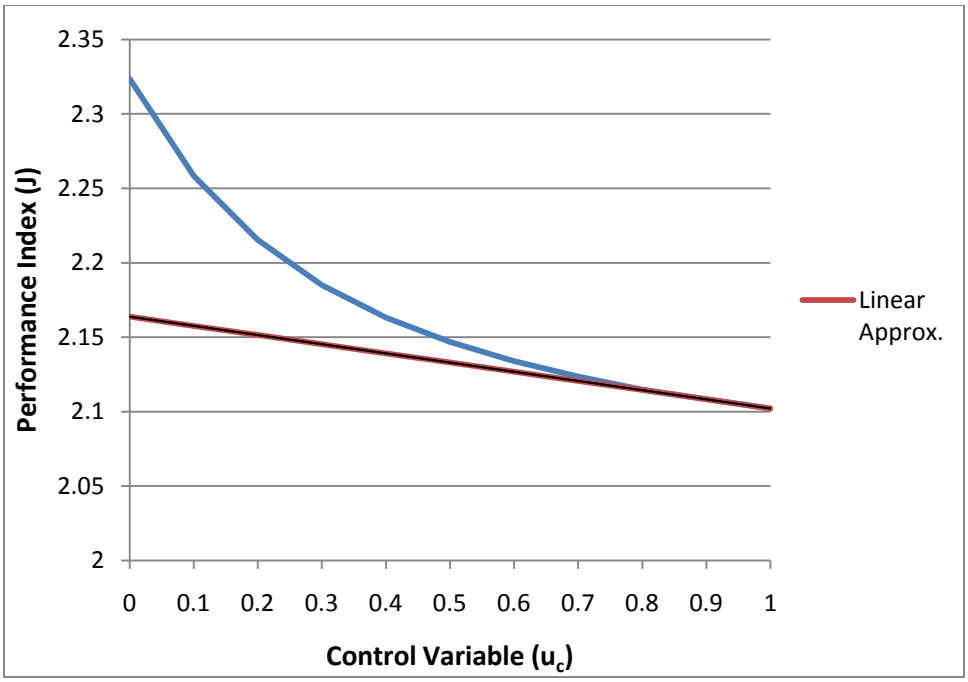

Figure 2.2. Nonlinear performance index (∝=1) for given circuit.

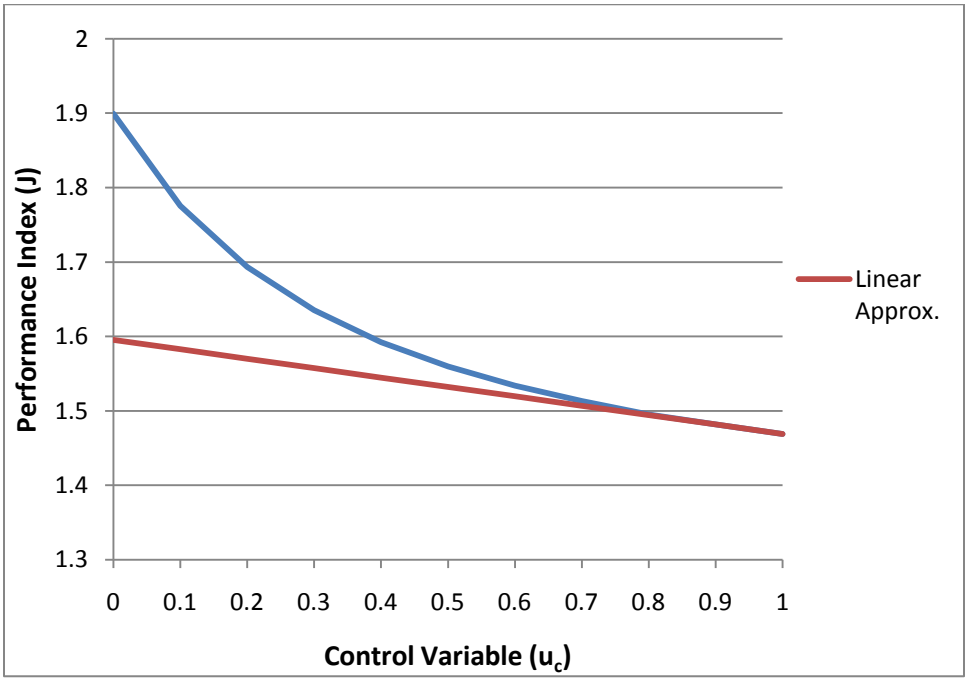

Figure 2.3. Nonlinear performance index (∝=2) for given circuit.

The proposed performance index definition claims that the linear approximations in Figure 2.2 and Figure 2.3 could be improved if the structure of the performance index were more linear (i.e. less nonlinear). The proposed performance index definition is shown in (2.3) as the difference between two performance indices, which are each defined in (2.4). In (2.4), J_{over} gives the index definition for the overloads of the given transmission line, and J_{margin} gives the index definition for the margin of the given transmission line. The definition of y_β for the overloads and margins takes the form of three equations as shown in (2.5), respectively. The variables k and m denote any two buses that are connected, and $z_{\beta,a}$ and $z_{\beta,b}$ are variables that will be explained in detail in Chapter 6 along with the explanation for the origination of these equations. While some terms are still nonlinear, the equations are at most of quadratic form, and this proposed method using the equations shown in (2.5) gives a more linearized structure of the performance index than the previous definition. This proposed definition will allow for the linear approximation found for the same single-line contingency (between Bus 1 and Bus 2) to be a more accurate indicator of the behavior of the performance index of the system for this outage.

$$J = J_{over} - J_{margin} \tag{2.3}$$

$$\begin{cases} J_{over} = \sum_n y_\beta \; ; \; y_\beta = max\{{I_\beta}^2 - {I_{\beta,0}}^2, 0\} \\ J_{margin} = \sum_n y_\beta \; ; \; y_\beta = min\{{I_\beta}^2 - {I_{\beta,0}}^2, 0\} \end{cases} \tag{2.4}$$

$$\begin{cases} y_\beta \pm {z_{\beta,a}}^2 = {I_\beta}^2 - {I_{\beta,0}}^2 \\ y_\beta \pm {z_{\beta,b}}^2 = 0 \\ z_{\beta,a} z_{\beta,b} = 0 \end{cases} \tag{2.5}$$

The results of applying this proposed index to the same transmission line (between Bus 1 and Bus 2) are given in Figures 2.4 – 2.5. The resulting overloading index is shown in Figure 2.4 where the blue line indicates the actual behavior of the performance index, and the red line shows the linear approximation using the pre-contingency slope. Also, the resulting index for the transmission line's margin is shown in Figure 2.5 with the red line again being the linear approximation of the blue index. The graph for the line's overload (Figure 2.4) has an upward (positive) slope since it is a result of the max function as shown in (2.4), and the graph for the margin of the line (Figure 2.5) has a downward (negative) slope due to the min function as given in (2.4).

The combination of the overload and margin of the line, given as the difference in accordance with (2.3), can be seen in Figure 2.6. The red line shows the overall linear approximation, and the blue line shows the true behavior of the performance index. The graph shown in Figure 2.6 has similar shape as both of those shown in Figure 2.2 and Figure 2.3 since it is a result of the maximum function so the result is positive, with an upward slope. Similarly, the other two indices result in only positive quantities since they consist of quantities that are raised to even powers. Since the overload PI is only slightly more linear than the case where $\propto = 1$, the values for the PI curve are similar for the two graphs, but the slopes of their linear approximations are slightly different since the slope for the overload PI is greater than that of the more nonlinear approximation. As the shape of the PI curve indicates, there is still some nonlinear behavior, which is expected since the equations used to define the index are not fully linear. However, since the equations are more linear than the previous definition and the slope of the approximating line is greater, the error of the linear approximation is less (2.5%) as determined using the formula shown in (2.2). Therefore, attempting to reduce the nonlinearities in the definition of the PI proves to reduce the error of the approximation, which leads to more accurate results from the contingency analysis process.

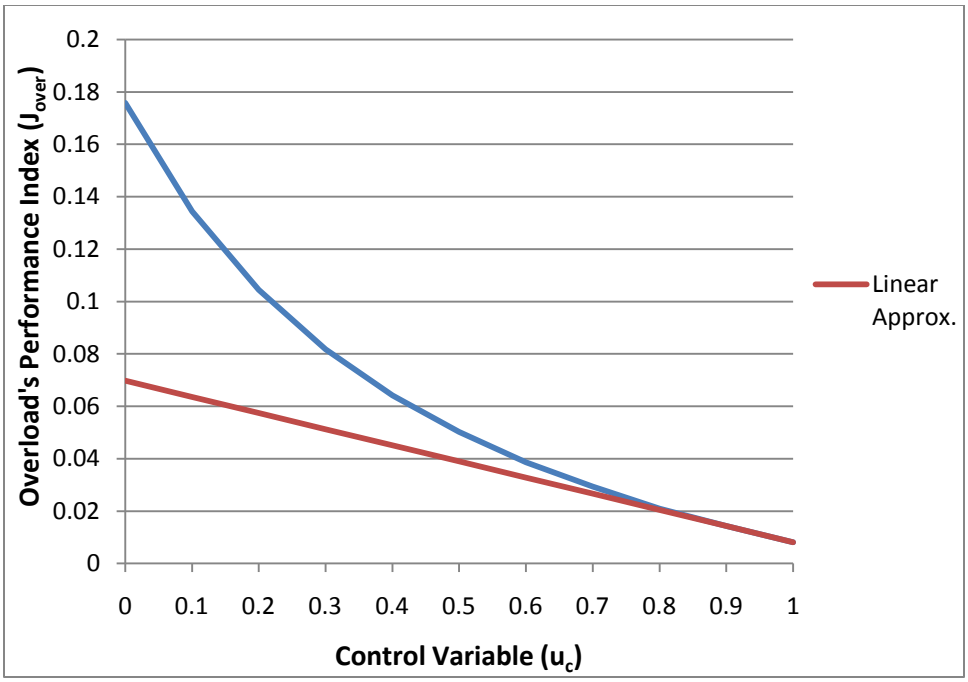

Figure 2.4. More linear performance index for the circuit's transmission overloads.

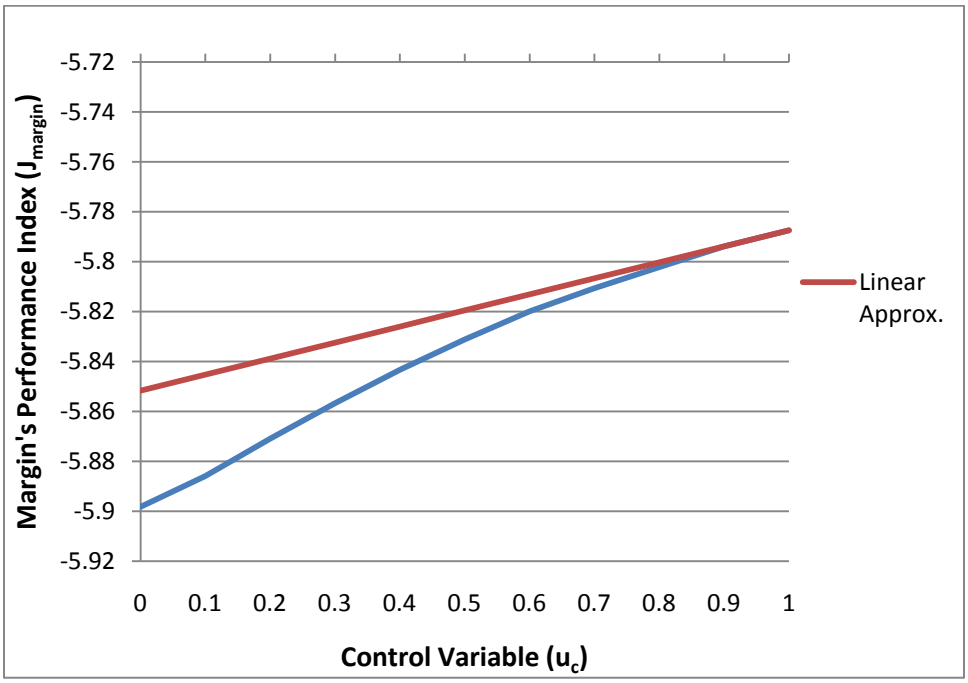

Figure 2.5. More linear performance index for the circuit's transmission margins.

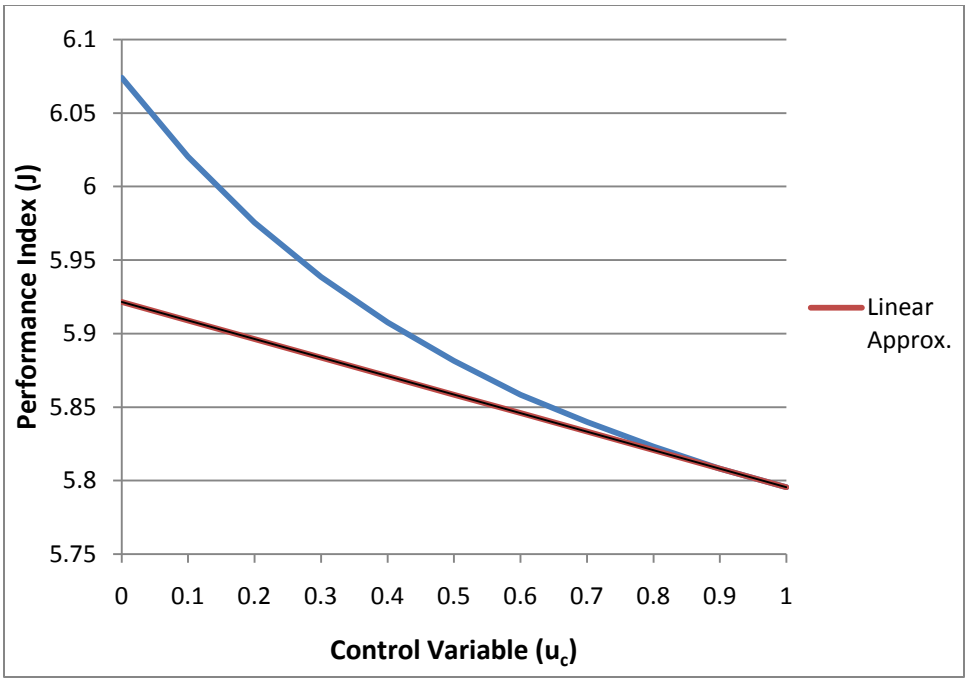

Figure 2.6. More linear performance index for the given circuit.

2.3 Future Modifications and Improvements

2.3.1 Improving Forecasting of Results for N-x Contingency Analysis

Since NERC requires only N-1 contingency operation, this research has focused only on N-1 (or, single) contingency operation. However, it is theoretically possible that a single contingency that may not be considered to be the most critical could lead to more catastrophic events than predicted from the N-1 contingency results. Therefore it is beneficial to be able to perform an N-x contingency analysis, where the 'x' represents the number of related contingencies that occur in succession, called cascading outages. Huang et al discuss the need for this type of analysis tool in [5] and also present the advantages of dynamic load balancing. Since the number of possible contingency cases grows exponentially with larger 'x' values, the calculations are significantly more

complex and time-consuming than the calculations required for N-1 calculations. However, in [5], the idea of dynamic load balancing among parallel processors is introduced in order to evenly distribute the work load to the available processors and achieve a higher calculation speed. This implementation still requires the security analysis to be carried out in each case, but it does theoretically allow for N-x contingency analysis in a more real-time setting where decisions must be made quickly.

2.3.2 Assisting Operators' Interpretation of Results

The operators who oversee the operation of power systems undergo many hundreds of hours of training, certifications, and work in a system of checks-and-balances to ensure the quality of their work and decisions they make. However, since the nature of the work of maintaining the security of a power system is time-critical, the operators still need additional help from the analysis programs to present the information in a straightforward and helpful manner. Hsu and Kuo explore the option of using fuzzy logic to help make decisions in the contingency ranking process based on the rules and guidelines the system operators use [6]. This addition to the current contingency selection process could speed the process for the operators because it helps make some of the decisions for them. Additionally, Bacher considers in [7] the idea of using visualization schemes to aid the operators in examining the results from the analysis. They claim that the operators will be able to interpret visual results more quickly than they will tabular results from the contingency ranking results [7]. Being able to visualize the results in this way could help make the most critical contingencies and problem areas more apparent to the operators more quickly.

2.3.3 Improving Computational Speed Using a Pre-filter

It has been proposed in [3] that the contingency selection part of the security analysis process can be viewed as a pre-filter for the contingency analysis since the contingency selection process allows only a small number of contingencies to continue to the next step of the analysis. By acting as a filter, contingency selection greatly decreases the computational effort needed to check all possible cases to find the worst contingency situations. The issue still remains, however, that there are a great number of contingencies that must be screened. Chen and Bose claim the contingencies that make it through the "filtering" process of contingency selection can be divided into three categories: critical, not critical, "not even marginally critical" [3]. They suggest a pre-filter design to separate the first two groups from the third group so that time is not spent computing results of contingencies that are "not even marginally critical" [3]. Combining this pre-filter technique with the current proposed method would decrease the time it takes to run all possible contingencies and produce a ranking of contingencies that more accurately reflects the actual performance of the system.

2.3.4 Additional Applications for Contingency Analysis

According to Musirin and Rahman, contingency analysis can be considered to be "a division" of voltage stability analysis and should be performed concurrently [8]. Voltage stability analysis uses a similar process as contingency analysis with a different performance index, which is instead called a "stability index" [9]. The purpose of voltage stability analysis is to help detect potential voltage collapse within the system. Since the contingencies considered during contingency analysis contribute greatly to the voltage stability outcome of the system, the results from the contingency analysis (e.g. load flow simulations) are used to compute the voltage stability index [9]. After the stability index has been calculated, the contingencies are then ranked according to which

ones have the most negative impact on the voltage stability of the system [9]. Therefore, the proposed contingency ranking method could help more accurately predict the behavior of a power system, which can be used to also improve results from the following voltage stability analysis.

2.4 Chapter Summary

The results from the example provided in Section 2.2 supports the assertion that a more linearized performance index will result in decreased error in the approximation of the index's curve. Using the proposed index, the linear approximation error is reduced by approximately 2.5% when compared with the approximation error of the more nonlinear index definition. Section 2.3 introduces several ways in which these more accurate results from contingency analysis can be incorporated into industry. Though the proposed research focuses on single-contingency analysis, Section 2.3.1 suggests a similar approach could be taken to linearize the performance index used to analyze 'x' number of linked contingencies. Section 2.3.2 provides details for how the computational speed of contingency analysis methods can be further improved to increase efficiency even more. Finally, according to Musirin and Rahman, as explained in Section 2.3.4, contingency analysis and voltage stability analysis can be performed concurrently, so this technique can also be applied to improve accuracy of the process of voltage stability analysis. Though the type of contingency analysis process is discussed in Section 2.1 and referenced throughout Section 2.3, specific details are not provided. Chapter 3 presents the structure of the contingency analysis process and the details for each step through the process.

CHAPTER 3

CONTINGENCY ANALYSIS OVERVIEW

Contingency analysis considers the response of the system with regard to an outage. For the purposes of this research, only individual outages are considered. With each individual outage, it is possible to solve the power flow for the state of the system with the element both in service and out of service, but it is too time-consuming. The process presented in this chapter uses the costate method to approximate the response of the system without solving for the state of the system for each individual outage.

3.1 The Contingency Analysis Process

Each element contingency has a control variable, u_c, associated with its status in the system. This control variable designates whether the element is in service or if it has been outaged and is defined as shown in (3.1). For instance, a pi-equivalent representation of a transmission line between two buses (Bus k and Bus m), shown in Figure 3.1, has its control variable modeled as a multiplier of the line's admittance and shunt components. When the control variable is one, the transmission line is in service and when it is zero, the transmission line has been outaged.

$$u_c = \begin{cases} 1.0 \text{ if the element is in service} \\ 0.0 \text{ if the element is outaged} \end{cases} \tag{3.1}$$

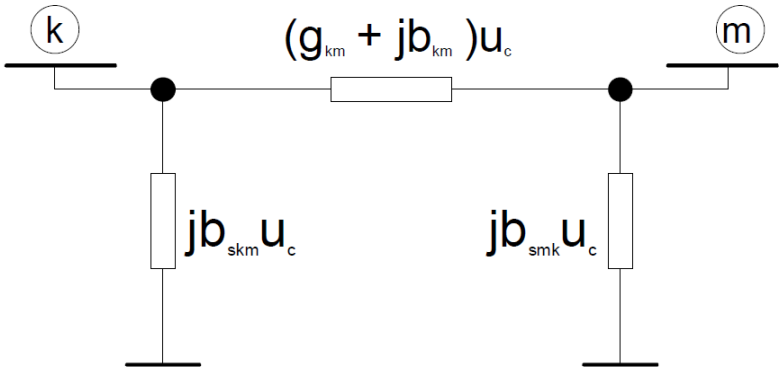

Figure 3.1. Pi-equivalent model of a transmission line with control variables [10].

The process of contingency analysis includes several steps where the ultimate goal is to calculate a value indicative of the change of the performance of the power system when a certain element is outaged. The performance index of the power system, J or f, with respect to each possible single element contingency, u_c, can be estimated by finding the slope, as shown in (3.2) [10]. The process of estimating the change in the performance index of the system is repeated for every possible contingency, c, as indicated in (3.2), so that the overall security of the system is known for any single contingency that could occur [10].

$$\Delta J = \frac{dJ}{du_c} \approx J(u_c = 0) \ \forall \ c \tag{3.2}$$

3.1.1 Calculation Process for ΔJ

The values for ΔJ can be calculated only after several other steps are first completed. The overall process is summarized in Figure 3.2, which shows that the process consists of three main parts. First, the state of the system must be solved, then a vector called the costate can be found. The costate vector, $\hat{\boldsymbol{x}}^{\boldsymbol{T}}$, gives the sensitivities of the state variables in the model and is invariant among all contingencies. Since the

costate vector is invariant, it is used in the third step to solve for ΔJ for every contingency.

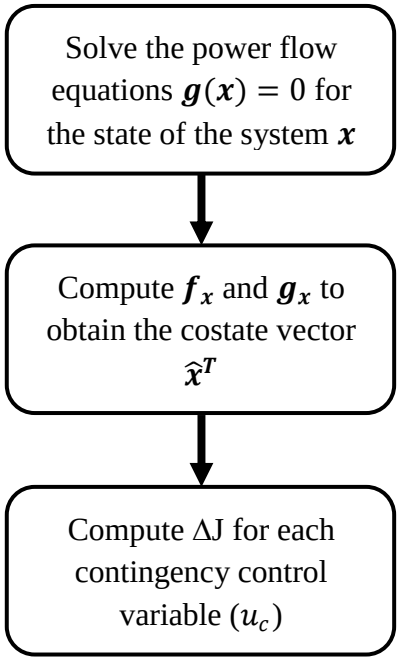

Figure 3.2 Block diagram of the process to calculate ΔJ.

Solving the State of the System

The first step consists of solving for the state of the system ($\boldsymbol{x}$) so that all voltages and currents are known in the system. The state of the system is solved using the power equations, $\boldsymbol{g}(\boldsymbol{x})$, which are defined in (3.3). These values need to be determined first because they are used throughout the rest of the calculations in the process. This process is iterative, and the Newton-Raphson Method, shown in (3.4), is used to converge to a solution for the system. The initial conditions of the system are taken as the values read from an input data file.

$$\boldsymbol{g}(\boldsymbol{x}) = 0 \tag{3.3}$$

$$\boldsymbol{x}_{n+1} = \boldsymbol{x}_n - \boldsymbol{g}(\boldsymbol{x}_n)\left(\frac{\partial \boldsymbol{g}(\boldsymbol{x}_n)}{\partial \boldsymbol{x}}\right)^{-1} \tag{3.4}$$

Calculating the Costate Vector

Next, the costate vector, $\widehat{\boldsymbol{x}}^{\boldsymbol{T}}$, is computed using the partial derivatives of the equations used to solve the state of the system ($\boldsymbol{g}_{\boldsymbol{x}}(\boldsymbol{x})$ or $\partial \boldsymbol{g}(\boldsymbol{x})/\partial \boldsymbol{x}$) and the partial derivatives of the performance index ($\boldsymbol{J}_{\boldsymbol{x}}$ or $\boldsymbol{f}_{\boldsymbol{x}}$) [10]. Equation 3.5 gives the formula used to find the costate vector [10]. The costate vector must be calculated only once, which minimizes the number of computations, and it can then be used to compute ΔJ for every control variable.

$$\widehat{\boldsymbol{x}}^{\boldsymbol{T}} = \boldsymbol{f}_{\boldsymbol{x}}\boldsymbol{g}_{\boldsymbol{x}}^{-\mathbf{1}} = \left(\frac{\partial f}{\partial \boldsymbol{x}}\right)\left(\frac{\partial \boldsymbol{g}(\boldsymbol{x})}{\partial \boldsymbol{x}}\right)^{-1} \tag{3.5}$$

Calculating ΔJ

After the costate vector is computed, the partial derivatives of the performance index and the power flow equations are calculated with respect to each control variable (J_u or f_u and $\boldsymbol{g}_u(\boldsymbol{x})$, respectively). Then the costate is used with the two partial derivative terms to determine ΔJ. Given the partial derivatives for each contingency control variable, the equation used to calculate ΔJ is given in (3.6) [10].

$$\Delta J = -\frac{dJ}{du_c} = (\widehat{\boldsymbol{x}}^{\boldsymbol{T}})(\boldsymbol{g}_{\boldsymbol{u}}(\boldsymbol{x})) - f_u \tag{3.6}$$

3.1.2 Estimating ΔJ

The value for ΔJ is estimated using a first order approximation given in (3.7) [10]. It is possible to directly calculate this value, but it becomes increasingly inefficient to do so with larger number of possible contingencies. However, using the linear approximation method can be useful and fairly accurate if the performance index being considered is of similar structure (i.e. near linear). The more linear the definition of the PI, the more accurate the first order approximation comes to predicting the behavior of the PI curve when each element is outaged.

$$\Delta J = J(u_c = 0) - J(u_c = 1) \tag{3.7}$$

3.2 Chapter Summary

This contingency analysis process Section 3.1.1 presents is used to approximate the response of the system when each element is outaged using a line. The linear approximation uses a point and a slope to approximate the nonlinear PI curve. The point is given by the initial state of the system (pre-contingency value of the PI), and the slope is given by the $\boldsymbol{\Delta J}$ term described in Section 3.1.2. The device equation models in the next chapter help to accurately describe the system using quadratic equations so that applying the contingency analysis process from this chapter produces accurate results in an efficient manner.

CHAPTER 4

QUADRATIZED POWER FLOW MODEL OVERVIEW

The QPF Model simplifies equations so that the solution to a set of equations can be found quickly. Each equation used in the QPF Model of the power system is of quadratic form and thus has variables with order no greater than two. Each element in the power system has a different set of equations that describes the behavior of that element using one (or multiple) quadratic equations to simulate an element's complex behavior in the system. The equations that model each element are developed first and are given in Section 4.1. These equations are re-arranged and combined in Chapter 6, which also gives more detail as to how these modeling equations for the different elements are combined.

4.1 The Quadratized Power Flow Model for Circuit Elements

The power flow equations are written in the form given in (3.3) so that the sum of all the terms is set equal to zero. Applying Kirchoff's Current Law (KCL), the QPF model uses the sum of all currents out of a single bus (e.g. Bus k). This idea is shown in (4.1) where m denotes any other bus in the system that is connected to Bus k. The current is divided into real and imaginary components in (4.2), and each of these parts can also be set equal to zero, as shown in (4.3). The current equations are primarily functions of the unknown voltages, which are also separated into real and imaginary components ($V_{k,real}$ and $V_{k,imag}$, respectively). The equations may also depend on other state variables that might come from additional equations necessary to accurately model certain equipment (e.g. generators and constant power loads). If any additional equations are needed, then these equations are added to the list of state equations in addition to the real and imaginary current equations.

$$\sum_{\forall m} \tilde{I}_{km} = 0 \tag{4.1}$$

$$\tilde{I}_{km} = I_{real} + jI_{imag} \tag{4.2}$$

$$\begin{cases} I_{km,real}\left(V_{k,real}, V_{k,imag}, \ldots\right) = 0 \\ I_{km,imag}\left(V_{k,real}, V_{k,imag}, \ldots\right) = 0 \end{cases} \tag{4.3}$$

4.1.1 Circuit Line Model

The circuit branches, or transmission lines, are represented using the pi-equivalent model shown in Figure 4.1. The model shows a transmission line between 'Bus k' and 'Bus m' with current flowing out of Bus k denoted as $\tilde{I}_{km}$ and current flowing out of Bus m denoted as $\tilde{I}_{mk}$. The y_{km}, y_{skm}, and y_{smk} terms denote the complex admittance and shunt elements along the line, respectively, where the two shunt elements are equal. The definition of y_{km} is given by (4.4), and the shunt elements are defined in (4.5). The equations used to calculate the currents flowing out of Bus k and out of Bus m, respectively, are shown in (4.6) with the series admittance and shunt terms taken into account appropriately [10]. The model and equations presented here are used to determine the current flowing through a circuit branch in the QPF solution technique.

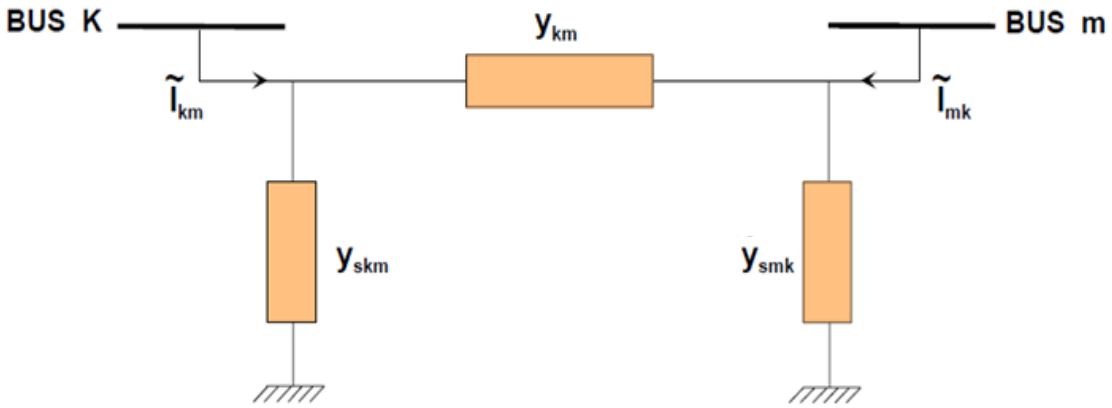

Figure 4.1. Circuit line pi-equivalent model [10].

$$y_{km} = g_{km} + jb_{km} \tag{4.4}$$

$$\frac{y_{skm}}{2} = \frac{y_{smk}}{2} = jB_{km} \tag{4.5}$$

$$\begin{cases} \tilde{I}_{km} = (y_{km} + y_{skm})\tilde{V}_k - y_{km}\tilde{V}_m \\ \tilde{I}_{mk} = -y_{km}\tilde{V}_k + (y_{km} + y_{smk})\tilde{V}_m \end{cases} \tag{4.6}$$

4.1.2 Generator Model

The generator model adds more complexity to the system, and as such, more than a single current equation is required to model a generator accurately. The equivalent circuit used to develop the generator equations is given in Figure 4.2. Figure 4.2 shows a generator attached to Bus k with bus voltage $\tilde{V}_k$, generator voltage $\tilde{E}_k$, generator admittance b_{gk}, and the current $\tilde{I}_k$, which is depicted as flowing out from the bus by convention. Both $\tilde{V}_k$ and $\tilde{E}_k$ are included in the state variables, or the solutions to the state power flow equations, and b_{gk} is given by the input file in pu. There are three modes in which generators function, and each mode requires a slightly different model to

accurately represent the behavior of the generator in the different modes. The three functioning modes of generators include Slack Mode, PQ Mode, and PV Mode.

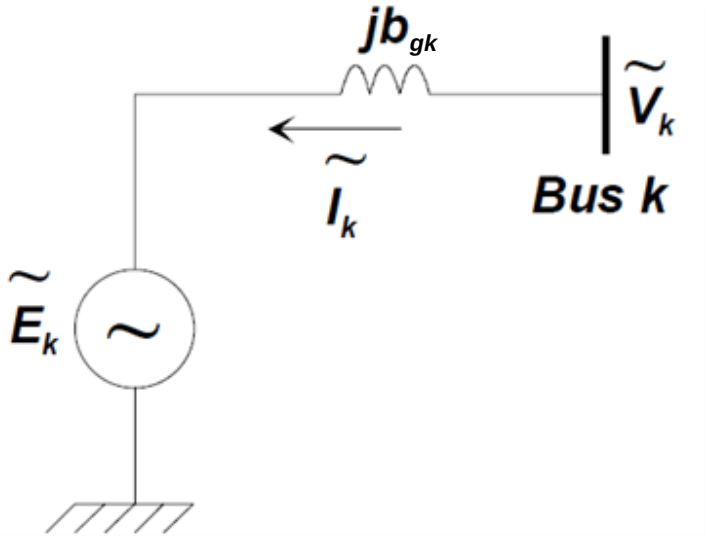

Figure 4.2. Generator equivalent circuit [10].

One mode that is not discussed in detail is a generator operating in Slack Mode. Generators connected to a slack bus operate in Slack Mode, but since the slack bus is neglected during analysis, these equations are not necessary. The other two modes for generators include PQ Mode and PV Mode. Generators operating in PQ Mode are attempting to hold constant the real and reactive power quantities, which are specified by the input file and represented as $P_{k,specified}$ and $Q_{k,specified}$, respectively. Generators operating in PV Mode attempt to hold constant the real power output as well as the voltage magnitude of the bus voltage, both of which are given by the input file ($P_{k,specified}$ and $V_{k,specified}$, respectively).

Both generator modes require a current equation, which is given in (4.7), but they also require additional equations, which differ depending on the mode [10]. The equation that requires the generated real and reactive power be held at a constant value for a

generator in PQ Mode is shown in (4.8) [10]. The equations that simulate constant real power being generated and a constant bus voltage, respectively, are given in (4.9) [10]. Equation 4.8 can also be separated into real and imaginary terms and thus split into two separate equations like the two given in (4.9) [10].

$$\tilde{I}_k = jb(\tilde{V}_k - \tilde{E}_k) \tag{4.7}$$

$$-jbV_k^2 + jb\tilde{V}_k\tilde{E}_k^* + P_{k,specified} + jQ_{k,specified} = 0 \tag{4.8}$$

$$\begin{cases} Re\{-jbV_k^2 + jb\tilde{V}_k\tilde{E}_k^*\} + P_{k,specified} = 0 \\ {V_{k,real}}^2 + {V_{k,imag}}^2 - {V_{k,specified}}^2 = 0 \end{cases} \tag{4.9}$$

4.1.3 Constant Power Load Model

Another element in the system that adds complexity is a constant power load, shown in Figure 4.3. The constant power load model simulates a load that draws constant real power from Bus k. The current $\tilde{I}_{dk}$ is designated as going out from the bus, and the generalized load is represented by $P_{dk} + jQ_{dk}$. The current equation is given in (4.10) where $Y_{dn,k}$ is the complex, nominal load admittance and u_{1k} is an additional state variable that appears in the additional equations given in (4.11) [10]. The nominal admittance $Y_{dn,k}$ is defined in (4.12) using the bus voltage magnitude and the conjugate of the load current $\tilde{I}_{dk}$ [10]. These equations also introduce another state variable u_{2k}, which is used to ensure the correct voltage at Bus k (lower equation of (4.11)), while the upper equation confirms that the real power part of the load is kept constant. The variables u_{1k} and u_{2k} are introduced to impose the correct behavior on the bus load. From previous QPF solutions, a typical value for u_{1k} is a small scalar (approximately 0.1) and u_{2k} is approximately 1.0.

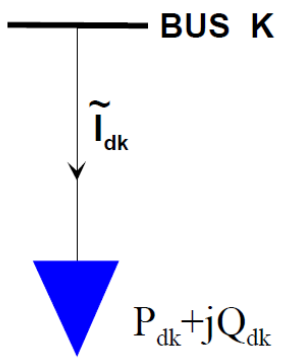

Figure 4.3. Constant Power Load equivalent circuit components [10].

$$\tilde{I}_{dk} = Y_{dn,k}\tilde{V}_k(1+u_{1k}) \tag{4.10}$$

$$\begin{cases} g_{dn,k}u_{2k}(1+u_{1k}) - P_{dk} = 0 \\ u_{2k} - ({V_{k,real}}^2 + {V_{k,imag}}^2) = 0 \end{cases} \tag{4.11}$$

$$Y_{dn,k} = g_{dn,k} + jb_{dn,k} = \left(\frac{1}{{V_{k,real}}^2 + {V_{k,imag}}^2}\right)(P_{dk} - jQ_{dk}) \tag{4.12}$$

4.2 Chapter Summary

This chapter presents the quadratic models for each element of the power system considered in this research. Section 4.1 provides the models used in the solution process for the three primary different devices using quadratic systems of equations: transmission line (Section 4.1.1), generator (Section 4.1.2), and constant power bus load (Section 4.1.3). Some of the variables in these equations are state variables that will be determined after solving the state of the system, which is the first step of the contingency analysis process as discussed in Section 3.1.1 of Chapter 3. The majority of the state variables in these equations are provided by an input file, however, and the initial values

for the bus voltage magnitudes are also provided in the input file. The format of the input file and information that it provides is presented in Chapter 5.

CHAPTER 5

INPUT FILE FORMAT

The input file provides all initial conditions and necessary data regarding the power system. The Power Technologies Incorporated (PTI) power flow data format and the Institute of Electrical and Electronics Engineers' (IEEE) Common Data Format (CDF) are among the most popular and widely used formats for sharing power flow data. In fact, the Northeast Power Coordinating Council (NPCC) specifically states in their data capture procedures that "[t]he preferred method for transferring system information is in PTI […] or IEEE common format" [11]. Therefore, selecting one of the two common formats arbitrarily, the PTI format serves as a relevant and useful choice for the input data format. This chapter presents the details of the PTI format (Section 5.1) and gives all formulas used to transform the data to the units required by the equations described generally in Chapter 4 and in more detail in Chapter 6.

5.1 PTI Data Format

The PTI format gives data divided into several sections, the first four of which are used during this research: Case Identification Data, Bus Data, Generator Data, and Branch Data. A description of this format is provided by a website hosted by The University of Washington's College of Engineering [12]. Some of the data must be modified, but the modifications are mostly trivial since the majority can be accomplished through simple, scalar division.

5.1.1 Case Identification Data Information

The header of the file gives the Case Identification Data, which consists of only a few lines. The only piece of useful information from this section of the file is the three-phase MVA base for the system, referred to as $SBASE$ in [12].

5.1.2 Bus Data Information

The Bus Data section is the first large data section of the file. The data used from this section include the bus number (I), bus type (IDE), bus real and reactive load (PL and QL, respectively), shunt susceptance and conductance at the bus (GL and BL, respectively), and the voltage magnitude and angle (VM and VA, respectively) [12]. The bus numbers are not required to be given in any particular order. Whatever order given for the bus numbers dictates the ordering of the real and imaginary current equations used to form the state power flow equations when solving the state of the system. The bus real and reactive load information (PL and QL, respectively) is given in MW and MVAR, so the $SBASE$ quantity given in the Case Identification Data is used to convert these values to a per unit base for the calculations and analysis as shown in (5.1). The shunt conductance and susceptance quantities are given in per unit, so these values can be used directly. Similarly, the voltage magnitude is also given in per unit, and the voltage angle (VA) is given in degrees, so the only conversion necessary to use these values is converting the angle to radians (5.2).

$$PL + jQL\ [pu] = \frac{PL\ [MW] + jQL\ [MVAR]}{SBASE\ [MVA]} \tag{5.1}$$

$$VA[rad] = VA[deg]\left(\frac{\pi\ [rad]}{180\ [deg]}\right) \tag{5.2}$$

5.1.3 Generator Data Information

The Generator Data section follows the Bus Data section and lists only the buses that have generators connected directly to them and all pertinent information about the generation at that bus [12]. The data used from this section include the bus number (I), the machine identifier (ID), generator's real and reactive generation (PG and QG, respectively), the voltage setpoint (VS), the generator regulation type as PQ or PV mode ($IREG$), the generator's MVA base ($MBASE$), the impedance of the generator (ZR and ZX), and the status of the generator ($STAT$) [12]. The bus number matches the bus numbers given in the Bus Data section so that the elements for the generator's current contributions can be added to the current equations at the appropriate bus. The machine identifier distinguishes between machines if there is more than one generator on a single bus. The real and reactive generation are given in MW and MVAR, respectively, so that these values must be converted into per unit using $MBASE$ or $SBASE$ before analysis (5.3). The voltage setpoint is given on a per unit base and is used only if the generator is operating in PV mode. The operation mode of the generator is indicated by $IREG$ such that a zero value indicates a generator that controls its voltage (PV mode) and a value of one indicates the generator is operating in PQ mode to control the real and reactive power generated. The three-phase power base of the machine is given in MVA by $MBASE$, and if there is no base given for the machine, the value defaults to the system base, $SBASE$, as indicated in the conversion to per unit shown in (5.3). The machine impedance is given in per unit, so it may be used directly. The status of the generator is given by $STAT$ such that a value of one ($STAT = 1$) means the generator is in service, and a value of zero means the generator is out of service. If a machine is out of service ($STAT = 0$), its contributions are not counted towards the current at its bus and no additional equations as given in (4.8) and (4.9) are added to the state equations of the system.

$$PG + jQG\ [pu] = \frac{PG\ [MW] + jQG\ [MVAR]}{MBASE\ [MVA]\ (\text{OR}\ SBASE\ [MVA])} \tag{5.3}$$

5.1.4 Branch Data Information

The Branch Data section follows the Generator Data section and contains information regarding all the connections of the system's buses and the information about each of those connections. The data used from this section includes the "from" and "to" bus numbers of each circuit ($Bus\ k$ and $Bus\ m$, respectively), the circuit identifier (CKT), the resistance of the line (R), the reactance of the line (X), the shunt terms of the pi-equivalent model (B), the MVA rating of the line ($RATEA$), and the status of the line (ST) [12]. The "from" and "to" bus numbers each correspond to the bus numbers given in the Bus Data section, and this information ensures that the components of each branch contribute only to the equations corresponding to the current at these two buses. The "from" bus is considered to be Bus k, and the "to" bus is referenced as Bus m. The "from" and "to" bus information is denoted by the subscripts for the parameters.

The resistance and reactance are both given in per unit and must be converted to their corresponding admittance values as shown in (5.4). The admittance parameters can be simplified to give the conductance (5.5) and susceptance (5.6) terms that can be used in the power flow equations in (4.6) to solve for the state of the system. The shunt terms of the line are already given in per unit, but they must be divided by two before applying them to the equations, as seen in (4.5). The power rating of the line is given in MVA, but this value is simply converted to per unit using the system power base ($SBASE$). The status of each circuit is defined to be zero if the branch is out of service and one if the branch is in service. Only the branches in service ($ST = 1$) can contribute terms for the state equations.

$$Y_{km} = g_{km} + jb_{km} = \frac{1}{Z_{km}} = \frac{1}{R + jX} = \frac{(R - jX)}{R^2 + X^2} \tag{5.4}$$

$$g_{km} = \frac{R}{R^2 + X^2} \tag{5.5}$$

$$jb_{km} = j\left(\frac{-X}{R^2 + X^2}\right) \tag{5.6}$$

5.2 Chapter Summary

This chapter describes how the data from the input file is applied to the equations used to model the system. The PTI format is broken into four main parts that are used for this research: Case Identification Data, Bus Data, Generator Data, and Branch Data. The majority of the required information is contained in the last three sections, and the only useful piece of information from the Case Identification Data section is the system's power rating. The contents of the three larger sections are described in more detail in Section 5.1.2 (Bus Data), Section 5.1.3 (Generator Data), and Section 5.1.4 (Branch Data). Now that there is a general understanding for the process of contingency analysis (Chapter 3), the QPF model (Chapter 4), and the origin and transformation of the system's input data (Chapter 5), the details of the formulation of the problem can be shown. Chapter 6 presents the detailed problem formulation used in this work.

CHAPTER 6

PROBLEM DEFINITION AND FORMULATION

Using the QPF model from Chapter 4 to describe a power system and the process of contingency analysis as presented in Chapter 3 leads to many sets of systems of equations that are involved in the solution process. It is necessary that a specific structure be defined so that these equations are handled in a similar manner. The structure of the state variables and state equations govern the structure of the partial derivative vectors and Jacobian matrices used to determine the state of the system, costate vector, and the approximated linear slope of the PI curve. This chapter presents the specific structure of these vectors throughout the contingency analysis process.

6.1 Performance Index Definition

The performance index, J, of the proposed method considers the combination of overloads and margins of elements with respect to their given ratings [13]. In particular, the performance index for transmission lines in a system is given in (6.1) where the y_{km} terms are defined for the overloads and margins, respectively, in (6.2) [13]. The variables k and m represent the "from" and "to" bus for a given circuit between Bus k and Bus m. The range of k from zero to n-1 and m from k+1 to n is used to denote all possibly connected buses and thus all circuits within the system since n represents the number of buses in the system. In this proposed index given in (6.1), the overloads and margins are defined based on the difference between the square of the current in a particular line and the square of the current rating of that line. The terms are each squared in order to make the partial derivatives of the terms with respect to the state variables be of order no greater than two, so the terms used in the Jacobian matrices are also quadratic. The

method presented in this chapter is carried out using a program written in C++ code by the author and using Dr. Cokkinides' *CSpatrix* matrix class [14], which is discussed in more detail in Appendix A.

$$J = f = \left(\sum_{\substack{k=0 \\ m=k+1}}^{n-1,n} y_{km,over} \right) - \left(\sum_{\substack{k=0 \\ m=k+1}}^{n-1,n} y_{km,margin} \right) \tag{6.1}$$

$$\begin{cases} y_{km,over} = max\{{I_{km}}^2 - {I_{km,0}}^2, 0\} \\ y_{km,margin} = min\{{I_{km}}^2 - {I_{km,0}}^2, 0\} \end{cases} \tag{6.2}$$

6.1.1 Solving for the y_{km} terms

Since the max and min functions are not quadratic equations themselves, they must be simulated using a set of quadratic equations as given in (6.3) for the overloads and (6.4) for the margins [13]. The variables z_{1km} and z_{2km} are introduced to restrict the value of y_{km} to be the maximum or minimum values as defined in (6.2) (for overloads and margins, respectively), where the value of either $z_{km,a}$ or $z_{km,b}$ will always be zero [13]. For the overloads, the variables $z_{km,a}$ and $z_{km,b}$ approximate the max function by requiring $z_{km,a}$ to be zero if the difference ${I_{km}}^2 - {I_{km,0}}^2$ is positive and non-zero otherwise and requiring $z_{km,b}$ to be non-zero if the difference ${I_{km}}^2 - {I_{km,0}}^2$ is positive and zero otherwise. Similarly for the margins, the variables $z_{km,a}$ and $z_{km,b}$ approximate the min function by requiring $z_{km,a}$ to be zero if the difference ${I_{km}}^2 - {I_{km,0}}^2$ is negative and non-zero otherwise and requiring $z_{km,b}$ to be non-zero if the difference ${I_{km}}^2 - {I_{km,0}}^2$ is negative and zero otherwise. Solving the systems of equations for y_{km} for the overloads and margins yields (6.5) and (6.6) for the overloads and margins, respectively.

The structure of y_{km} shown in (6.5) and (6.6) is used in the formulation of J as a quadratic equation.

$$\begin{cases} y_{km} - z_{km,a}^2 = {I_{km}}^2 - {I_{km,0}}^2 \\ y_{km} - z_{km,b}^2 = 0 \\ z_{km,a} z_{km,b} = 0 \end{cases} \tag{6.3}$$

$$\begin{cases} y_{km} + {z_{km,a}}^2 = {I_{km}}^2 - {I_{km,0}}^2 \\ y_{km} + {z_{km,b}}^2 = 0 \\ z_{km,a} z_{km,b} = 0 \end{cases} \tag{6.4}$$

$$y_{km} = \frac{1}{2}\left[\left({z_{km,a}}^2 + {z_{km,b}}^2\right) + \left({I_{km}}^2 - {I_{km,0}}^2\right)\right] \tag{6.5}$$

$$y_{km} = \frac{1}{2}\left[-\left({z_{km,a}}^2 + {z_{km,b}}^2\right) + \left({I_{km}}^2 - {I_{km,0}}^2\right)\right] \tag{6.6}$$

6.1.2 Calculating the I_{km}^2 terms

The complex term $\tilde{I}_{km}$, given by (4.6), can be split into real and imaginary admittance and voltage components as shown in (6.7). Equation 6.7 can be further simplified to obtain real and imaginary current components as given in (6.8), which can be combined as in (6.9) and (6.10) to give the ${I_{km}}^2$ rating term for each circuit. The real and imaginary voltage values for Bus k and Bus m ends of the line ($V_{k,real}$, $V_{k,imag}$ and $V_{m,real}$, $V_{m,imag}$, respectively) become state variables, and the ${I_{km}}^2$ term becomes a quadratic function of the voltages, which is necessary for the QPF model.

$$\begin{aligned}\tilde{I}_{km} &= (g_{km} + jb_{km} + jB_{km})\left(V_{k,real} + jV_{k,imag}\right) \\ &\quad - (g_{km} + jb_{km})\left(V_{m,real} + jV_{m,imag}\right)\end{aligned} \tag{6.7}$$

$$\begin{cases} I_{km,real} = g_{km}V_{k,real} - (b_{km} + B_{km})V_{k,imag} - g_{km}V_{m,real} + b_{km}V_{m,imag} \\ I_{km,imag} = (b_{km} + B_{km})V_{k,real} + g_{km}V_{k,imag} - b_{km}V_{m,real} - g_{km}V_{m,imag} \end{cases} \tag{6.8}$$

$$I_{km}{}^2 = I_{km,real}{}^2 + I_{km,imag}{}^2 \tag{6.9}$$

$$\begin{aligned} I_{km}{}^2 &= \left(g_{km}{}^2 + b_{km}{}^2\right)\left(V_{k,real} - V_{m,real}\right)^2 + 2(b_{km} + B_{km})^2 V_{k,imag}{}^2 \\ &\quad + \left(g_{km}{}^2 + b_{km}{}^2\right)V_{m,imag}{}^2 \\ &\quad + 2(b_{km} - g_{km})(b_{km} + B_{km})\left(V_{k,real} - V_{m,real}\right)V_{k,imag} \\ &\quad - 2(g_{km} + b_{km})(b_{km} + B_{km})V_{k,imag}\,V_{m,imag} \end{aligned} \tag{6.10}$$

6.1.3 Calculating the $I_{km,0}{}^2$ terms

The $I_{km,0}{}^2$ terms in (6.3) and (6.4) are easily computed since the MVA rating of the line ($RATEA$) value is given by the input file. Since the value imported from the input file is given in MVA, the value must be converted to per unit using the three-phase system power base ($SBASE$). The system power base is also given in the input file, though, so this conversion is simple after the data has been read from the file and before calculations are made.

6.2 Solving for the State of the System

In order to solve for the state of the given power system, there are two main combinations of input data that must be processed. Before any components for calculations can be made, the structure of the state variables of the system, x, (i.e. the values the process attempts to find), must be defined. The order of these variables

defines the structure of the two main components. The first main component is a vector of the state equations, $\boldsymbol{g}(\boldsymbol{x})$, which are based on the topology of the system and the QPF model for the branches, generators, and bus loads as given in Chapter 4. Next, the Jacobian matrix ($\boldsymbol{g}_{\boldsymbol{x}}(\boldsymbol{x})$ or $\partial \boldsymbol{g}(\boldsymbol{x})/\partial \boldsymbol{x}$) is formed, which is the partial derivative of each of the power flow equations with respect to the state variables. The Jacobian uses the same order of the power flow equations and state variables vectors. After these components are calculated, the iterative process of Newton-Raphson Method (3.4) starts to converge on a final solution, whose values are used in the following analysis.

6.2.1 Forming the State Power Flow Equations

The power flow equations include the sum of the real and imaginary current components at each bus and any additional equations required by generators and constant power loads at buses. There are current equation contributions from the QPF generator and bus load models, so the current equations from these elements must be combined with the branch circuit equations.

Branch Equations

The branch equations that contribute to the power flow equations are composed of current equations only. Equation 4.7 gave the phasor representation of the current from Bus k along the circuit branch from Bus k to Bus m. This complex representation can be divided into real and imaginary components, which are given in (6.8) in terms of the circuit elements (admittance and shunt terms).

Generator Equations

The generator equations contain both current equations and two additional equations depending on the mode of the generator. The complex current equation given in (4.7) can be divided into real and imaginary current components, which are given in

(6.11). The equations in (6.11) are written in terms of the admittance of the generator (b_{gk}), the real and imaginary components of the generator's voltage ($E_{k,real}$ and $E_{k,imag}$, respectively), and the real and imaginary components of the bus voltage ($V_{k,real}$ and $V_{k,imag}$, respectively) to which the generator is connected.

$$\begin{cases} I_{k,real} = b_{gk}\left(E_{k,imag} - V_{k,imag}\right) \\ I_{k,imag} = b_{gk}\left(V_{k,real} - E_{k,real}\right) \end{cases} \tag{6.11}$$

PQ Mode Generator

A generator operating in PQ Mode has two additional equations that come from expanding (4.8) into real and imaginary components as shown in (6.12). The equations in (6.12) consider the same variables as the current equations in (6.11) and use additionally the values of the specified real and reactive power ($P_{k,specified}$ and $Q_{k,specified}$, respectively) that are to be maintained by the generator.

$$\begin{cases} b_{gk}\left(V_{k,real}\,E_{k,imag} - V_{k,imag}\,E_{k,real}\right) + P_{k,specified} = 0 \\ b_{gk}\left[\left(V_{k,real}\,E_{k,real} + V_{k,imag}\,E_{k,imag}\right) - \left({V_{k,real}}^2 + {V_{k,imag}}^2\right)\right] + Q_{k,specified} = 0 \end{cases} \tag{6.12}$$

PV Mode Generator

A generator operating in PV Mode needs two additional equations as given in (4.9). The equations can be simplified by solving for the real part of the expression given in the top equation and are shown in (6.13). The equations in (6.13) consider the same variables as the current equations in (6.11) and also require the values of the specified real power and bus voltage ($P_{k,specified}$ and $V_{k,specified}$, respectively) that are to be maintained by the generator.

$$\begin{cases} b_{gk}\left(V_{k,real}\,E_{k,imag} - V_{k,imag}\,E_{k,real}\right) + P_{k,specified} = 0 \\ {V_{k,real}}^2 + {V_{k,imag}}^2 - {V_{k,specified}}^2 = 0 \end{cases} \tag{6.13}$$

Bus Load Equations

Similar to the generator equations, the model for the constant power bus load requires both real and imaginary current component equations and two additional equations. The complex current equation given in (4.10) can be divided into real and imaginary current components, which are given in (6.14). The equations in (6.14) are written in terms of the nominal load conductance and susceptance (g_{dnk} and b_{dnk}, respectively), the state variable u_{1k}, and the bus real and imaginary voltage components ($V_{k,real}$ and $V_{k,imag}$, respectively). The two additional equations in (4.11) also apply and are restated in (6.15) for convenience where u_{2k} is a state variable and P_{dk} is the real load power. The additional variables u_{1k} and u_{2k} will be referred to as the "u-variables."

$$\begin{cases} I_{dk,real} = (1+u_{1k})\left(g_{dnk}V_{k,real} - b_{dnk}V_{k,imag}\right) \\ I_{dk,imag} = (1+u_{1k})\left(b_{dnk}V_{k,real} + g_{dnk}V_{k,imag}\right) \end{cases} \tag{6.14}$$

$$\begin{cases} g_{dn,k}u_{2k}(1+u_{1k}) - P_{dk} = 0 \\ u_{2k} - ({V_{k,real}}^2 + {V_{k,imag}}^2) = 0 \end{cases} \tag{6.15}$$

6.2.2 Structure of the State Variables Vector

The state variables include all non-specified parameters from the power flow equations. From the QPF model of a circuit branch between Bus k and Bus m, the real and imaginary components of the Bus k voltages are unknown ($V_{k,real}$ and $V_{k,imag}$, respectively) as well as the real and imaginary components of the Bus m voltages ($V_{m,real}$ and $V_{m,imag}$, respectively). From the QPF model of a generator at Bus k (either mode PQ or PV), the unknown variables include the real and imaginary components of the voltage at Bus k ($V_{k,real}$ and $V_{k,imag}$, respectively) and the real and imaginary components of the generator voltage ($E_{k,real}$ and $E_{k,imag}$, respectively). From the QPF model of a constant power bus load at Bus k, the unknown variables include the real and imaginary

components of the voltage at Bus k ($V_{k,real}$ and $V_{k,imag}$, respectively) and the u-variables (u_{1k} and u_{2k}). The state variables ($\boldsymbol{x}$) are therefore arranged as shown in (6.16). This notation assumes the slack bus is considered to be Bus 0 and there are n buses so that the real and imaginary bus voltage components listed include V_1 through V_{n-1}. Furthermore, it is assumed that the number of generators is g so that the number of generators included are E_1 through E_{g-1}. Lastly, it is also assumed that the number of constant power bus loads is d so that the u-variables listed include u_1 through u_{d-1}. It should be noted that the notation of E_1 and u_1 does not necessarily require there to be a generator and/or bus load at the same bus that corresponds to V_1; it is simply an indication of the first generator listed in the input file and the first bus listed with a bus load, respectively.

$$\begin{bmatrix} \boldsymbol{x}_1 = V_{1,real} \\ \boldsymbol{x}_2 = V_{1,imag} \\ \vdots \\ \boldsymbol{x}_{2n-1} = V_{n-1,real} \\ \boldsymbol{x}_{2n} = V_{n-1,imag} \\ \boldsymbol{x}_{2n+1} = E_{1,real} \\ \boldsymbol{x}_{2n+2} = E_{1,imag} \\ \vdots \\ \boldsymbol{x}_{2n+2g-1} = E_{g-1,real} \\ \boldsymbol{x}_{2n+2g} = E_{g-1,imag} \\ \boldsymbol{x}_{2n+2g+1} = u_{1,1} \\ \boldsymbol{x}_{2n+2g+2} = u_{1,2} \\ \vdots \\ \boldsymbol{x}_{2n+2g+2d-1} = u_{d-1,1} \\ \boldsymbol{x}_{2n+2g+2d} = u_{d-1,2} \end{bmatrix} \tag{6.16}$$

6.2.3 Structure of the State Equations Vector

Current Equations

Since all elements of the power system have components that contribute to the current at the buses to which they are connected, they must all be added in order to apply

KCL. As shown in Figure 6.1, at each bus there could be one or more transmission lines connected, an equivalent generator, and an equivalent bus load with current directions defined as they were in the QPF model for each element and as shown in Figure 6.1. The term "equivalent" used to describe generators and bus loads at a bus refers to the fact that multiple of either element type at a single bus can be combined to form one equivalent element of each type. Since all currents are defined as pointing out of the bus in Figure 6.1, the sum of these currents must be zero according to KCL and as demonstrated in (6.17). Although there is only one transmission line model shown in Figure 6.1, there could be several, which is accounted for in (6.17) with the sum of all $\tilde{I}_{km}$ for any line to any Bus m that is connected from Bus k. Equation 6.17 is reduced to give the power flow equations at each bus for the real and imaginary current components as shown in (6.18). Applying the real and imaginary current contributions from the QPF models for a circuit branch (6.8), generator (6.11), and bus load (6.14) gives a final form as shown in (6.19) for the real and (6.20) for imaginary components.

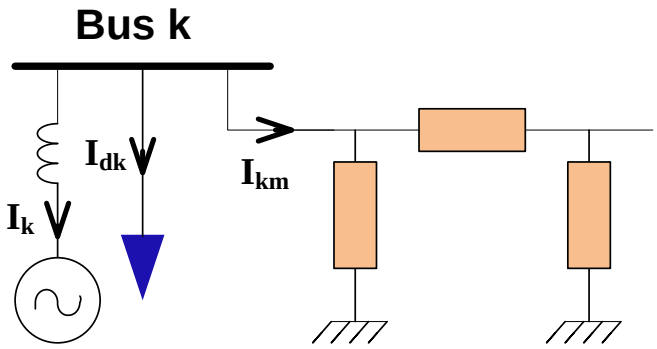

Figure 6.1. Combination of QPF Model's currents at Bus k.

$$\sum \tilde{I}_k = \left(\sum_{\forall m} \tilde{I}_{km}\right) + (\tilde{I}_{dk}) + (\tilde{I}_k) = 0 \qquad (6.17)$$

$$\begin{cases} \sum I_{k,real} = \left(\sum_{\forall m} I_{k,real}\right) + \left(I_{dk,real}\right) + \left(I_{k,real}\right) = 0 \\ \sum I_{k,imag} = \left(\sum_{\forall m} I_{k,imag}\right) + \left(I_{dk,imag}\right) + \left(I_{k,imag}\right) = 0 \end{cases} \tag{6.18}$$

$$\begin{aligned} \sum I_{k,real} = \Bigg[\sum_{\forall m} & g_{km} V_{k,real} - (b_{km} + B_{km}) V_{k,imag} - g_{km} V_{m,real} \\ & + b_{km} V_{m,imag}\Bigg] + \left[b_{gk}\left(E_{k,imag} - V_{k,imag}\right)\right] \\ & + \left[(1 + u_{1k})\left(g_{dnk} V_{k,real} - b_{dnk} V_{k,imag}\right)\right] \end{aligned} \tag{6.19}$$

$$\begin{aligned} \sum I_{k,imag} = \Bigg[\sum_{\forall m} & (b_{km} + B_{km}) V_{k,real} + g_{km} V_{k,imag} - b_{km} V_{m,real} \\ & - g_{km} V_{m,imag}\Bigg] + \left[b_{gk}\left(V_{k,real} - E_{k,real}\right)\right] \\ & + \left[(1 + u_{1k})\left(b_{dnk} V_{k,real} + g_{dnk} V_{k,imag}\right)\right] \end{aligned} \tag{6.20}$$

Additional Equations

The additional equations in the list of state equations follow the current equations for all the buses. These additional equations come from the generators and bus loads in the system as given in (6.12) and (6.13) for the generators (PQ and PV, respectively) and in (6.15) for the bus loads.

Overall Structure

The overall structure for the state equations vector ($\boldsymbol{g}(\boldsymbol{x})$) is shown in (6.21) as a combination of the current equations and the additional equations. The vector's structure is divided into three groups: current equations, additional generator equations, and

additional bus load equations. As seen in (6.21) , the current equations for all currents flowing from all buses (except the slack bus) are listed first, followed by all generator additional equations second, which is followed by the additional bus load equations for each bus load given at the end. This structure parallels the structure of the state variables given in (6.16). Also similar to the notation in (6.16), there are assumed to be n buses, g generators (includes both PQ and PV types), and d constant power bus loads. The subscripts of the generators and bus load equations do not correspond to the matching current equations but simply indicate the position of the generator and bus load relative to each group. Also, the second equation for each additional generator equation G_κ depends on the mode, is listed separately and is given in (6.22) for $\kappa = \{1, \dots, (g-1)\}$.

$$\begin{bmatrix} \boldsymbol{g}_1(\boldsymbol{x}) = \sum I_{1,real} = 0 \\ \boldsymbol{g}_2(\boldsymbol{x}) = \sum I_{1,imag} = 0 \\ \vdots \\ \boldsymbol{g}_{2n-1}(\boldsymbol{x}) = \sum I_{n-1,real} = 0 \\ \boldsymbol{g}_{2n}(\boldsymbol{x}) = \sum I_{n-1,imag} = 0 \\ \boldsymbol{g}_{2n+1}(\boldsymbol{x}) = b_{g1}\left(V_{1,real}\, E_{1,imag} - V_{1,imag}\, E_{1,real}\right) + P_{1,specified} = 0 \\ \boldsymbol{g}_{2n+2}(\boldsymbol{x}) = G_1 = 0 \\ \vdots \\ \boldsymbol{g}_{2n+2g-1}(\boldsymbol{x}) = b_{g,g-1}\left(V_{g-1,real}\, E_{g-1,imag} - V_{g-1,imag}\, E_{g-1,real}\right) + P_{g-1,specified} = 0 \\ \boldsymbol{g}_{2n+2g}(\boldsymbol{x}) = G_{g-1} = 0 \\ \boldsymbol{g}_{2n+2g+1}(\boldsymbol{x}) = g_{dn,1} u_{2,1}\left(1 + u_{1,1}\right) - P_{dn,1} = 0 \\ \boldsymbol{g}_{2n+2g+2}(\boldsymbol{x}) = u_{2,1} - \left({V_{1,real}}^2 + {V_{1,imag}}^2\right) = 0 \\ \vdots \\ \boldsymbol{g}_{2n+2g+2d-1}(\boldsymbol{x}) = g_{dn,d-1} u_{2,d-1}\left(1 + u_{1,d-1}\right) - P_{dn,d-1} = 0 \\ \boldsymbol{g}_{2n+2g+2d}(\boldsymbol{x}) = u_{2,d-1} - \left({V_{d-1,real}}^2 + {V_{d-1,imag}}^2\right) = 0 \end{bmatrix} \tag{6.21}$$

$$G_\kappa = \left\{ b_{g\kappa}\left[\left(V_{\kappa,real}\, E_{\kappa,real} + V_{\kappa,imag}\, E_{\kappa,imag}\right) - \left({V_{\kappa,real}}^2 + {V_{\kappa,imag}}^2\right)\right] + Q_{\kappa,specified} \right\} \text{ or } \left\{ {V_{\kappa,real}}^2 + {V_{\kappa,imag}}^2 - {V_{\kappa,specified}}^2 \right\} \tag{6.22}$$

6.2.4 Structure of the Jacobian Matrix

The Jacobian matrix ($\boldsymbol{g_x(x)}$) contains the partial derivatives of all state equations with respect to all state variables. Each row is given as shown in (6.23) for values of $\kappa = \{1, \dots, (2n + 2g + 2d)\}$. The Jacobian matrix is square with size $(2n + 2g + 2d)$. The first $(2n \times 2n)$ terms are denser than the rest of the matrix, but the matrix overall is quite sparse with mostly entries of zero.

$$\boldsymbol{g_{x,\kappa}(x)} = \left[\frac{\partial \boldsymbol{g}_\kappa(\boldsymbol{x})}{\partial \boldsymbol{x}_1} \quad \frac{\partial \boldsymbol{g}_\kappa(\boldsymbol{x})}{\partial \boldsymbol{x}_2} \quad \dots \quad \frac{\partial \boldsymbol{g}_\kappa(\boldsymbol{x})}{\partial \boldsymbol{x}_{2n+2g+2d-1}} \quad \frac{\partial \boldsymbol{g}_\kappa(\boldsymbol{x})}{\partial \boldsymbol{x}_{2n+2g+2d}}\right] \tag{6.23}$$

6.3 Solving for the Costate Vector

The costate vector ($\boldsymbol{\hat{x}^T}$) also requires the state equations vector ($\boldsymbol{g(x)}$) and state variables vector ($\boldsymbol{x}$) but additionally requires the PI definition, as shown in (3.5). Specifically, the vector of partial derivatives of the performance index with respect to the state variables ($\boldsymbol{f_x}$) and the matrix of partial derivatives of the state equations with respect to the state variables ($\boldsymbol{g_x(x)}$), are used to calculate the costate vector. Though the state equations and Jacobian use the same terminology as was used when solving for the state of the system, the set of state equations in this part of the process are augmented. The set of state equations also now includes a set of three equations (referred to as the "y,z equations") for every branch. This set of three equations are required in order to reproduce the max and min functions used in the definition of the PI and are given in (6.3) for the overloads definition and (6.4) for the margins definition.

From this point in the solution process moving forward, there are two separate calculations made – one for the overloads and one for the margins. Most of the values do not change, but they must be kept separate since the definitions of each PI are not completely equal. The only difference between the two index definitions is the sign (+ or –) before the z variables in the y,z equations [10].

6.3.1 Additional y,z Equations from Performance Index Definition

The y,z equations are added to the previous set of state equations to give the new, augmented state equations. The equations given in (6.21) remain without any changes and are listed before the y,z equations. The set of y,z equations added to each set of state equations will depend on whether the definition is for the overloads or margins index. The PI for the overloads will include y,z equations of the form given in (6.3) at the end of the state equations vector, while the PI for the margins will include y,z equations of the form given in (6.4).

6.3.2 Structure of the State Variables Vector

The state variables vector in this section of calculations ($\boldsymbol{x_{PI}}$) includes all the variables given in (6.16) since all the state equations used previously also apply now. It is also augmented to include variables from the y,z equations at the end. Since the variables in each set of y,z equations are the same for each PI definition, it is the same for both the overloads and the margins and is shown in (6.24). All the same assumptions are made (n buses, g generators, d bus loads), and additionally, it is assumed there are β branches. Similarly, the notation for the subscripts of the y and z variables indicates only the connection between the first and second buses that are connected and does not necessarily indicate the buses whose bus voltage real and imaginary components corresponding to V_1 and V_2 are connected. For example, if the first three buses listed in the input data file's Bus Data Information section are given as "Bus 10," "Bus 20," and "Bus 30," their bus magnitude variables would be $V_{10,real}$ and $V_{10,imag}$ for Bus 10, $V_{20,real}$ and $V_{20,imag}$ for Bus 20, and $V_{30,real}$ and $V_{30,imag}$ for Bus 30. In the Branch Data Information section of the input file, Bus 10 and Bus 20 may not be connected, so it may be that the first connection listed is between Bus 20 and Bus 30. Using the described notation, the variable $y_{1,2}$ would refer to the connection between Bus 20 and Bus 30,

although Bus 20 and Bus 30 are not the first and second buses, respectively, that are listed in the Bus Data Information section.

$$\begin{bmatrix} \boldsymbol{x_{PI},}_{1} = V_{1,real} \\ \boldsymbol{x_{PI},}_{2} = V_{1,imag} \\ \vdots \\ \boldsymbol{x_{PI},}_{2n-1} = V_{n-1,real} \\ \boldsymbol{x_{PI},}_{2n} = V_{n-1,imag} \\ \boldsymbol{x_{PI},}_{2n+1} = E_{1,real} \\ \boldsymbol{x_{PI},}_{2n+2} = E_{1,imag} \\ \vdots \\ \boldsymbol{x_{PI},}_{2n+2g-1} = E_{g-1,real} \\ \boldsymbol{x_{PI},}_{2n+2g} = E_{g-1,imag} \\ \boldsymbol{x_{PI},}_{2n+2g+1} = u_{1,1} \\ \boldsymbol{x_{PI},}_{2n+2g+2} = u_{1,2} \\ \vdots \\ \boldsymbol{x_{PI},}_{2n+2g+2d-1} = u_{d-1,1} \\ \boldsymbol{x_{PI},}_{2n+2g+2d} = u_{d-1,2} \\ \boldsymbol{x_{PI},}_{2n+2g+2d+1} = y_{1,2} \\ \boldsymbol{x_{PI},}_{2n+2g+2d+2} = z_{1,2,a} \\ \boldsymbol{x_{PI},}_{2n+2g+2d+3} = z_{1,2,b} \\ \vdots \\ \boldsymbol{x_{PI},}_{2n+2g+2d+3\beta-2} = y_{\beta-2,\beta-1} \\ \boldsymbol{x_{PI},}_{2n+2g+2d+3\beta-1} = z_{\beta-2,\beta-1,a} \\ \boldsymbol{x_{PI},}_{2n+2g+2d+3\beta} = z_{\beta-2,\beta-1,b} \end{bmatrix} \quad (6.24)$$

6.3.3 Structure of the Contingency State Equations Vector

The new set of state equations for the overloads and margins must both be augmented to include the corresponding y,z equations. The set of state equations for the overloads ($\boldsymbol{g_{over}}(\boldsymbol{x_{PI}})$) are given in (6.25), and the set of state equations for the margins ($\boldsymbol{g_{margin}}(\boldsymbol{x_{PI}})$) are given in (6.26). In the row $\boldsymbol{g_{over}}_{,2n+2g-1}(\boldsymbol{x_{PI}})$ of (6.25), the term $P_{g-1,specified}$ is shortened to $P_{g-1,spec}$ for space-saving reasons. Similarly, in (6.26), the row $\boldsymbol{g_{mar}}_{,2n+2g-1}(\boldsymbol{x_{PI}})$ has the same simplification, and additionally, the subscript "margin" is shortened to "mar." The shortened subscript is also used in (6.26) for the row $\boldsymbol{g_{mar}}_{,2n+2g+2d+3\beta-2}(\boldsymbol{x_{PI}})$.

$$
\begin{bmatrix}
\boldsymbol{g_{over,1}}(\boldsymbol{x_{PI}}) = \sum I_{1,real} = 0 \\
\boldsymbol{g_{over,2}}(\boldsymbol{x_{PI}}) = \sum I_{1,imag} = 0 \\
\vdots \\
\boldsymbol{g_{over,2n-1}}(\boldsymbol{x_{PI}}) = \sum I_{n-1,real} = 0 \\
\boldsymbol{g_{over,2n}}(\boldsymbol{x_{PI}}) = \sum I_{n-1,imag} = 0 \\
\boldsymbol{g_{over,2n+1}}(\boldsymbol{x_{PI}}) = b_{g1}\left(V_{1,real}\, E_{1,imag} - V_{1,imag}\, E_{1,real}\right) + P_{1,specified} = 0 \\
\boldsymbol{g_{over,2n+2}}(\boldsymbol{x_{PI}}) = G_1 = 0 \\
\vdots \\
\boldsymbol{g_{over,2n+2g-1}}(\boldsymbol{x_{PI}}) = b_{g,g-1}\left(V_{g-1,real}\, E_{g-1,imag} - V_{g-1,imag}\, E_{g-1,real}\right) + P_{g-1,spec} = 0 \\
\boldsymbol{g_{over,2n+2g}}(\boldsymbol{x_{PI}}) = G_{g-1} = 0 \\
\boldsymbol{g_{over,2n+2g+1}}(\boldsymbol{x_{PI}}) = g_{dn,1} u_{2,1}\left(1 + u_{1,1}\right) - P_{dn,1} = 0 \\
\boldsymbol{g_{over,2n+2g+2}}(\boldsymbol{x_{PI}}) = u_{2,1} - \left({V_{1,real}}^2 + {V_{1,imag}}^2\right) = 0 \\
\vdots \\
\boldsymbol{g_{over,2n+2g+2d-1}}(\boldsymbol{x_{PI}}) = g_{dn,d-1} u_{2,d-1}\left(1 + u_{1,d-1}\right) - P_{dn,d-1} = 0 \\
\boldsymbol{g_{over,2n+2g+2d}}(\boldsymbol{x_{PI}}) = u_{2,d-1} - \left({V_{d-1,real}}^2 + {V_{d-1,imag}}^2\right) = 0 \\
\boldsymbol{g_{over,2n+2g+2d+1}}(\boldsymbol{x_{PI}}) = y_{1,2} - {z_{1,2,a}}^2 - \left({I_{1,2}}^2 - {I_{1,2,0}}^2\right) = 0 \\
\boldsymbol{g_{over,2n+2g+2d+2}}(\boldsymbol{x_{PI}}) = y_{1,2} - {z_{1,2,b}}^2 = 0 \\
\boldsymbol{g_{over,2n+2g+2d+3}}(\boldsymbol{x_{PI}}) = z_{1,2,a} z_{1,2,b} = 0 \\
\vdots \\
\boldsymbol{g_{over,2n+2g+2d+3\beta-2}}(\boldsymbol{x_{PI}}) = y_{\beta-2,\beta-1} - {z_{\beta-2,\beta-1,a}}^2 - \left({I_{\beta-2,\beta-1}}^2 - {I_{\beta-2,\beta-1,0}}^2\right) = 0 \\
\boldsymbol{g_{over,2n+2g+2d+3\beta-1}}(\boldsymbol{x_{PI}}) = y_{\beta-2,\beta-1} - {z_{\beta-2,\beta-1,b}}^2 = 0 \\
\boldsymbol{g_{over,2n+2g+2d+3\beta}}(\boldsymbol{x_{PI}}) = z_{\beta-2,\beta-1,a} z_{\beta-2,\beta-1,b} = 0
\end{bmatrix} \tag{6.25}
$$

$$
\begin{bmatrix}
\boldsymbol{g_{margin,1}(x_{PI})} = \sum I_{1,real} = 0 \\
\boldsymbol{g_{margin,2}(x_{PI})} = \sum I_{1,imag} = 0 \\
\vdots \\
\boldsymbol{g_{margin,2n-1}(x_{PI})} = \sum I_{n-1,real} = 0 \\
\boldsymbol{g_{margin,2n}(x_{PI})} = \sum I_{n-1,imag} = 0 \\
\boldsymbol{g_{margin,2n+1}(x_{PI})} = b_{g1}\left(V_{1,real}\, E_{1,imag} - V_{1,imag}\, E_{1,real}\right) + P_{1,specified} = 0 \\
\boldsymbol{g_{margin,2n+2}(x_{PI})} = G_1 = 0 \\
\vdots \\
\boldsymbol{g_{mar,2n+2g-1}(x_{PI})} = b_{g,g-1}\left(V_{g-1,real}\, E_{g-1,imag} - V_{g-1,imag}\, E_{g-1,real}\right) + P_{g-1,spec} = 0 \\
\boldsymbol{g_{margin,2n+2g}(x_{PI})} = G_{g-1} = 0 \\
\boldsymbol{g_{margin,2n+2g+1}(x_{PI})} = g_{dn,1} u_{2,1}\left(1 + u_{1,1}\right) - P_{dn,1} = 0 \\
\boldsymbol{g_{margin,2n+2g+2}(x_{PI})} = u_{2,1} - \left({V_{1,real}}^2 + {V_{1,imag}}^2\right) = 0 \\
\vdots \\
\boldsymbol{g_{margin,2n+2g+2d-1}(x_{PI})} = g_{dn,d-1} u_{2,d-1}\left(1 + u_{1,d-1}\right) - P_{dn,d-1} = 0 \\
\boldsymbol{g_{margin,2n+2g+2d}(x_{PI})} = u_{2,d-1} - \left({V_{d-1,real}}^2 + {V_{d-1,imag}}^2\right) = 0 \\
\boldsymbol{g_{margin,2n+2g+2d+1}(x_{PI})} = y_{1,2} + {z_{1,2,a}}^2 - \left({I_{1,2}}^2 - {I_{1,2,0}}^2\right) = 0 \\
\boldsymbol{g_{margin,2n+2g+2d+2}(x_{PI})} = y_{1,2} + {z_{1,2,b}}^2 = 0 \\
\boldsymbol{g_{margin,2n+2g+2d+3}(x_{PI})} = z_{1,2,a} z_{1,2,b} = 0 \\
\vdots \\
\boldsymbol{g_{mar,2n+2g+2d+3\beta-2}(x_{PI})} = y_{\beta-2,\beta-1} + {z_{\beta-2,\beta-1,a}}^2 - \left({I_{\beta-2,\beta-1}}^2 - {I_{\beta-2,\beta-1,0}}^2\right) = 0 \\
\boldsymbol{g_{margin,2n+2g+2d+3\beta-1}(x_{PI})} = y_{\beta-2,\beta-1} + {z_{\beta-2,\beta-1,b}}^2 = 0 \\
\boldsymbol{g_{margin,2n+2g+2d+3\beta}(x_{PI})} = z_{\beta-2,\beta-1,a} z_{\beta-2,\beta-1,b} = 0
\end{bmatrix} \tag{6.26}
$$

6.3.4 Structure of the Contingency Jacobian Matrix

The Jacobian matrix ($\boldsymbol{g_{x_{PI}}(x_{PI})}$), like the state equations and state variables, is also augmented by the additional y,z equations in this part of the solution process since the state equations and state variables have been augmented. There are also two Jacobian matrices that must be formed – one for the case of the overloads ($\boldsymbol{g_{over,x_{PI}}(x_{PI})}$) and one for the margins ($\boldsymbol{g_{margin,x_{PI}}(x_{PI})}$). As before, the Jacobian is a square matrix, but here its size is $(2n + 2g + 2d + 3\beta)$. The structure for row κ of the Jacobian for the overloads PI is given in (6.27), and the structure for the margins PI is given in (6.28) where $\kappa = \{1, \dots, (2n + 2g + 2d + 3\beta)\}$. Like the previous Jacobian, this one is also

extremely sparse with the section $(2n \times 2n)$ still being the densest in the matrix. The subscripts in (6.28) are shortened to "mar" instead of "margin."

$$\boldsymbol{g}_{\boldsymbol{over},\boldsymbol{x}_{\boldsymbol{PI}},\kappa}(\boldsymbol{x}_{\boldsymbol{PI}}) = \left[\frac{\partial \boldsymbol{g}_{\boldsymbol{over},\kappa}(\boldsymbol{x}_{\boldsymbol{PI}})}{\partial \boldsymbol{x}_{\boldsymbol{PI},1}} \quad \frac{\partial \boldsymbol{g}_{\boldsymbol{over},\kappa}(\boldsymbol{x}_{\boldsymbol{PI}})}{\partial \boldsymbol{x}_{\boldsymbol{PI},2}} \quad \cdots \quad \frac{\partial \boldsymbol{g}_{\boldsymbol{over},\kappa}(\boldsymbol{x}_{\boldsymbol{PI}})}{\partial \boldsymbol{x}_{\boldsymbol{PI},2n+2g+2d+3\beta-1}} \quad \frac{\partial \boldsymbol{g}_{\boldsymbol{over},\kappa}(\boldsymbol{x}_{\boldsymbol{PI}})}{\partial \boldsymbol{x}_{\boldsymbol{PI},2n+2g+2d+3\beta}}\right] \quad (6.27)$$

$$\boldsymbol{g}_{\boldsymbol{margin},\boldsymbol{x}_{\boldsymbol{PI}},\kappa}(\boldsymbol{x}_{\boldsymbol{PI}}) = \left[\frac{\partial \boldsymbol{g}_{\boldsymbol{mar},\kappa}(\boldsymbol{x}_{\boldsymbol{PI}})}{\partial \boldsymbol{x}_{\boldsymbol{PI},1}} \quad \frac{\partial \boldsymbol{g}_{\boldsymbol{mar},\kappa}(\boldsymbol{x}_{\boldsymbol{PI}})}{\partial \boldsymbol{x}_{\boldsymbol{PI},2}} \quad \cdots \quad \frac{\partial \boldsymbol{g}_{\boldsymbol{mar},\kappa}(\boldsymbol{x}_{\boldsymbol{PI}})}{\partial \boldsymbol{x}_{\boldsymbol{PI},2n+2g+2d+3\beta-1}} \quad \frac{\partial \boldsymbol{g}_{\boldsymbol{mar},\kappa}(\boldsymbol{x}_{\boldsymbol{PI}})}{\partial \boldsymbol{x}_{\boldsymbol{PI},2n+2g+2d+3\beta}}\right] \quad (6.28)$$

6.4 Calculation of ΔJ for Contingencies

After the costate vector is calculated, the calculation of the value of ΔJ for each contingency case is relatively simple. The only elements left to find are the partial derivatives of the state equations (for both the overloads and the margins) with respect to each control variable ($\boldsymbol{g}_{\boldsymbol{over},u_c}(\boldsymbol{x}_{\boldsymbol{PI}})$ and $\boldsymbol{g}_{\boldsymbol{margin},u_c}(\boldsymbol{x}_{\boldsymbol{PI}})$, respectively) and the partial derivative of each PI with respect to each control variable. The partial derivatives of the state equations are in vector form, which is then multiplied by the costate vector to give a scalar result. The partial derivative of the performance indices for each control variable is a scalar already, so the difference of the two can be taken easily as seen in (3.6). As shown in Figure 3.1, the only terms affected by the control variables are the circuit branch contributions for both the state equations and the PI definitions.

6.4.1 Structure of df/du

The only circuit branch terms of each PI (overloads and margins) can be found in the ${I_{km}}^2$ term given in (6.5) for the overloads and (6.6) for the margins. With the control

variables explicitly included, the equation can be written as (6.29) and (6.30) (for overloads and margins, respectively) for each branch contingency for the branch between Bus k and Bus m. The control variable $u_{c(k,m)}$ is added to show the dependence of the equation on the control variable. Since these terms are the same for both the overloads and the margins, only one value is calculated. The form for each $f_{u_c}(\boldsymbol{x_{PI}})$ is therefore shown in (6.31) since the ${I_{km}}^2$ term is the only term with the contributions of the circuit branch components to the corresponding single branch contingency.

$$y_{km} = \frac{1}{2}\left[\left({z_{km,a}}^2 + {z_{km,b}}^2\right) + \left({u_{c,(k,m)}}^2\right)\left({I_{km}}^2{u_{km}}^2 - {I_{km,0}}^2\right)\right] \tag{6.29}$$

$$y_{km} = \frac{1}{2}\left[-\left({z_{km,a}}^2 + {z_{km,b}}^2\right) + \left({u_{c,(k,m)}}^2\right)\left({I_{km}}^2{u_{km}}^2 - {I_{km,0}}^2\right)\right] \tag{6.30}$$

$$f_{u_c}(\boldsymbol{x_{PI}}) = {I_{km}}^2 \tag{6.31}$$

6.4.2 Structure of dg/du

The $\boldsymbol{g}_{u_c}(\boldsymbol{x_{PI}})$ vector must be found for every contingency control variable u_c, and it is found by taking the partial derivatives of each state equation with respect to a given control variable. There are only five equations for each contingency where the control variable contributions can be found. Four of those equations that have control variable contributions for $u_{c(k,m)}$ (where the branch is from Bus k to Bus m) are those listed in the real and imaginary current components for both the "from" and the "to" side currents. These equations are found in (6.8) and are reformatted to show the dependence on $u_{c(k,m)}$ as shown in (6.32) for the "from" side real and imaginary current components, respectively. The subscripts are shortened to "r" instead of "real," and "i" instead of "imag" to save space. The fifth contribution of a given control variable $u_{c(k,m)}$ comes from the ${I_{km}}^2$ term in the y_{km} equation for the branch between Bus k and Bus m.

Rewriting (6.32) as (6.33) shows the ${I_{km}}^2$ term depends on the square of the control variable. Therefore the overall structure of $\boldsymbol{g}_{u_{c(k,m)}}(\boldsymbol{x_{PI}})$ for a given contingency on the branch between Bus k and Bus m is given in (6.34). The vector $\boldsymbol{g}_{u_{c(k,m)}}(\boldsymbol{x_{PI}})$ has size $\{(2n + 2g + 2d + 3\beta) \times 1\}$ with non-zero terms in the real and imaginary current equations corresponding to the k^{th} and m^{th} bus as well as the branch equation corresponding to the branch (k, m). The branch equation, which is the opposite sign of ${I_{k,m}}^2$, is too long to include in the vector but is defined explicitly in (6.10). Clearly, this vector is also sparse since only five terms are non-zero.

$$\begin{cases} I_{km,r} = u_{c(k,m)}\left[g_{km}V_{k,real} - (b_{km} + B_{km})V_{k,imag} - g_{km}V_{m,real} + b_{km}V_{m,imag}\right] \\ I_{km,i} = u_{c(k,m)}\left[(b_{km} + B_{km})V_{k,real} + g_{km}V_{k,imag} - b_{km}V_{m,real} - g_{km}V_{m,imag}\right] \end{cases} \tag{6.32}$$

$$\begin{aligned} {I_{km}}^2 = \left({u_{c(k,m)}}^2\right)\Big[&({g_{km}}^2 + (b_{km} + B_{km})^2)\left({V_{k,real}}^2 + {V_{k,imag}}^2\right) \\ &+ \left({g_{km}}^2 + {b_{km}}^2\right)\left({V_{m,real}}^2 + {V_{m,imag}}^2\right) \\ &- 2({g_{km}}^2 + b_{km}(b_{km} + B_{km}))\left(V_{k,real}V_{m,real}\right) \\ &- 2(g_{km}B_{km})\left(V_{k,real}V_{m,imag}\right) \\ &+ 2(g_{km}B_{km})\left(V_{k,imag}V_{m,real}\right) \\ &- 2({g_{km}}^2 + b_{km}(b_{km} + B_{km}))\left(V_{k,imag}V_{m,imag}\right)\Big] \end{aligned} \tag{6.33}$$

$$\begin{bmatrix} 0 \\ \vdots \\ 0 \\ \boldsymbol{g}_{u_{c(k,m)},k}(\boldsymbol{x_{PI}}) = g_{km}V_{k,real} - (b_{km} + B_{km})V_{k,imag} - g_{km}V_{m,real} + b_{km}V_{m,imag} \\ \boldsymbol{g}_{u_{c(k,m)},k+1}(\boldsymbol{x_{PI}}) = (b_{km} + B_{km})V_{k,real} + g_{km}V_{k,imag} - b_{km}V_{m,real} - g_{km}V_{m,imag} \\ 0 \\ \vdots \\ 0 \\ \boldsymbol{g}_{u_{c(k,m)},m}(\boldsymbol{x_{PI}}) = g_{km}V_{k,real} - (b_{km} + B_{km})V_{k,imag} - g_{km}V_{m,real} + b_{km}V_{m,imag} \\ \boldsymbol{g}_{u_{c(k,m)},m+1}(\boldsymbol{x_{PI}}) = (b_{km} + B_{km})V_{k,real} + g_{km}V_{k,imag} - b_{km}V_{m,real} - g_{km}V_{m,imag} \\ 0 \\ \vdots \\ 0 \\ \boldsymbol{g}_{u_{c(k,m)}2n+2g+2d+(k,m)}(\boldsymbol{x_{PI}}) = -I_{k,m}{}^2 \\ 0 \\ \vdots \\ 0 \end{bmatrix} \quad (6.34)$$

6.5 Chapter Summary

The solution approach this work presents goes through many stages that must be performed in the order that this chapter provides, which is shown in Figure 3.2. The proposed PI definition introduces many variables, and the details of how to work with these terms are given in Section 6.1. Section 6.2 discusses how the equations are all combined and shows the detailed structure of the vectors and matrices used in the first part of the analysis, which solves for the initial state of the system. The structure of the state variables and state equations vectors are provided in Section 6.2.2 and Section 6.2.3, respectively. Section 6.2.4 discusses the structure of the Jacobian used to solve for the initial state of the system and provides an example of the structure of one of the rows. Section 6.3 provides details as to how the augmented equations are combined to solve for the costate vector, which is necessary to solve for the slope used in the linear approximation for each contingency. Section 6.3.2 and Section 6.3.3 present the structure of the augmented state variables and state equations vectors for both the overloads and margins, and Section 6.3.4 explains the overall structure of the Jacobian

needed to obtain the costate vector and provides an example row for the Jacobian from both the overload and margin cases. Finally, Section 6.4 makes use of all the details presented in earlier sections so that the slope (ΔJ) for each contingency can be found, which is required to achieve the linear approximation for each contingency. Section 6.4.1 discusses the details of finding f_u for each contingency, and Section 6.4.2 discusses the details of finding $\boldsymbol{g}_u(\boldsymbol{x_{PI}})$ for each contingency, which are both required along with the costate vector to solve for the value ΔJ for each contingency. The solution method this chapter details is applied to a test system and results are presented in Chapter 7.

CHAPTER 7

TEST SYSTEM AND RESULTS

A small, four bus system is used to run initial tests to evaluate the utility of the proposed performance index. This system is used to compute performance index approximations for two different types of performance indices: two highly nonlinear ones and the proposed, quadratic (slightly more linear) definition. The results are presented graphically so that comparisons between the linear approximations and their corresponding PI curves can be made.

7.1 Test System

The two nonlinear PI definitions are shown in (7.1) where $\propto = \{1,2\}$, and the proposed, more linear method is shown in (7.2) where the y_{km} terms are defined in (7.3). Since the overload ($y_{km,over}$) and margin ($y_{km,margin}$) indices are complimentary of one another, the difference of the two is used instead of using either one individually.

$$J_{1,\propto} = \sum_{k,m} \left(\frac{I_{km}}{I_{km,0}} \right)^{2\propto} \tag{7.1}$$

$$J_2 = \sum_{k,m} \left(y_{km,over} - y_{km,margin} \right) \tag{7.2}$$

$$\begin{cases} y_{km,over} = max\{{I_{km}}^2 - {I_{km,0}}^2\} \\ y_{km,margin} = min\{{I_{km}}^2 - {I_{km,0}}^2\} \end{cases} \tag{7.3}$$

The test system is shown in Figure 7.1. The bus numbers are given inside circles next to each bus as Bus 1, Bus 2, Bus 3, and Bus 4. There are generators at Bus 1 and

Bus 2, with the generator at Bus 1 operating in slack mode and the generator at Bus 2 operating in PV mode. There is a constant power load drop at Bus 4. The transmission line parameters for this system are assumed to have no series conductance term (g_{km}) or shunt (B_{km}) terms.

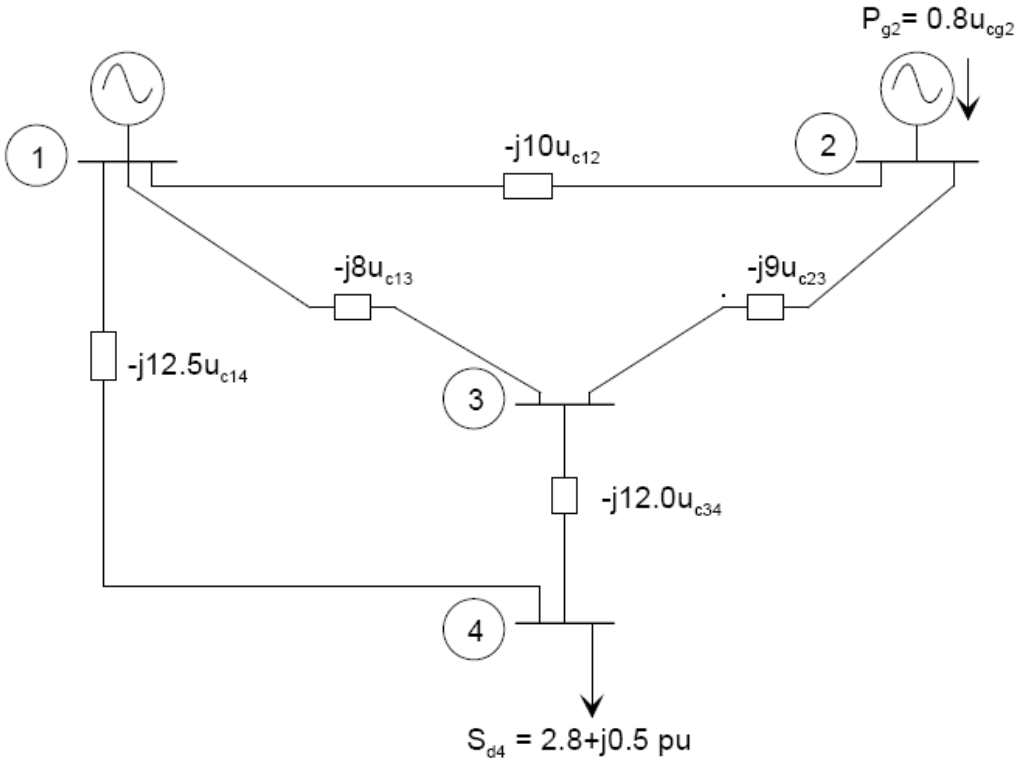

Figure 7.1. Four bus test system [10].

7.1.1 Test System's PTI Data File

The PTI file with the data for the system shown in Figure 7.1 is given in Table B.2. The actual input file text has commas between each item in each column, though, so that it is in Comma-Separated Values (CSV) format. The system base is given to be 100 MVA ($SBASE = 100MVA$), and there is no separate machine base given for the two generators ($MBASE = 0$), so the system base is used when converting the parameters to their per unit equivalents for calculations. The only other data given in the file that is not shown in Figure 7.1 are the MVA ratings for each line ($RATEA$), which are shown in

Table 7.1. Each of the five circuits in the system is also given a reference circuit number in Table 7.1.

Table 7.1. Test System Line Ratings [10].

From Bus	To Bus	Line Rating (MVA)	Circuit
1	2	110	1
1	3	110	2
1	4	250	3
2	3	110	4
3	4	110	5

7.1.2 Highly Nonlinear Performance Index Results

The linear approximation of each performance index is shown in comparison to the true behavior of the performance index for single branch contingencies for each highly nonlinear PI definition. Each contingency is simulated by allowing the control variable (u_c) to approach zero, which simulates the outage. The linear approximation uses a slope of ΔJ at the pre-contingency conditions (i.e. when $u_c = 1$) and shows how the linear approximation compares to the PI curve when the value of the control variable approaches zero.

The PI $J_{1,1}$ refers to the index when $\propto = 1$, and $J_{1,2}$ refers to the index when $\propto = 2$. The solution process uses the problem formulation presented in Chapter 6, except these two indices require no augmenting since there are no y-z equations in this case. Therefore, the state vector and power flow equations used to solve the state of the system are the same as those used to find the costate vector and solve for ΔJ in each definition for $J_{1,1}$ and $J_{1,2}$.

Performance Index $J_{1,1}$ ($\propto$=1)

The problem is formulated as described in Chapter 6, and the change in the performance index (ΔJ) is approximated for each circuit outage. Each result is shown

graphically to show how the linear approximation compared to the nonlinear PI curve. The data for these results is given in Table B.3 for the outages of circuits 1–5.

Circuit 1 Outage

The results when circuit 1 (between Bus 1 and Bus 2) is outaged are shown in Figure 7.2 where the blue line is the actual index's performance and the red line is the linear approximation. The slope of the linear approximation is slightly negative since the PI curve slopes upwards from the initial state of the system (pre-contingency), and it is specifically given to be $\Delta J = -0.06164$. The linear approximation estimates the outage with an error of almost 7%. Though the difference between the curves when $u_c = 0$ appears large in Figure 7.2, the scale is small so that the difference is on the order of 10^{-1}.

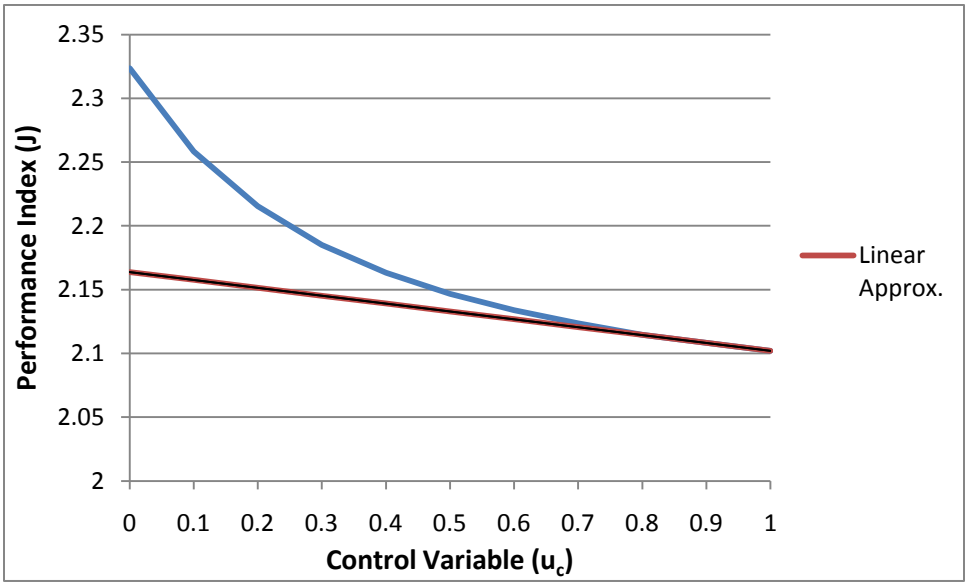

Figure 7.2. Results from circuit 1 outage for $J_{1,1}$.

Circuit 2 Outage

The results from the outage of circuit 2 (between Bus 1 and Bus 3) are shown in Figure 7.3 where the red line gives the linear approximation of the blue PI behavior with a calculated value of $\Delta J = 0.260452$. The PI curve initially slopes downward and turns up again when the circuit is completely outaged, but the overall result is below the initial state of the system so the slope of the line is positive. The linear approximation only deviates from the PI curve once the control variable's value drops below 0.5. Therefore, the difference for the case of an outage is only 0.1 even when the line is fully out of service, so the error for this approximation is around 5.5%.

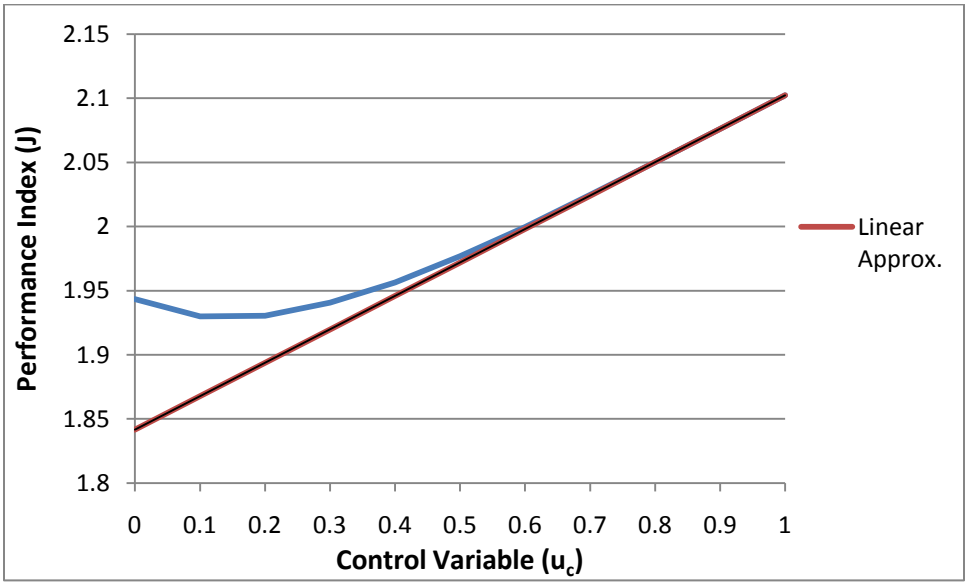

Figure 7.3. Results from circuit 2 outage for $J_{1,1}$.

Circuit 3 Outage

The results from the outage of circuit 3 (between Bus 1 and Bus 4) are shown in Figure 7.4 where the blue line shows the actual PI behavior, and the red line gives the linear approximation using $\Delta J = -1.55237$. The shape of this PI curve is similar to the one produced by the outage of circuit 1 except more dramatic since the PI curve for this

outage reaches a value of 17.5, while the curve in Figure 7.2 stays below 2.5 after the outage. The slope of the approximation for this outage is also negative with greater magnitude of the negative slope for the outage of circuit 1. The difference between the approximation and the PI curve grows quickly after the control variable's value falls below 0.7, and the overall error for the approximation of the outage of circuit 3 is almost 80%.

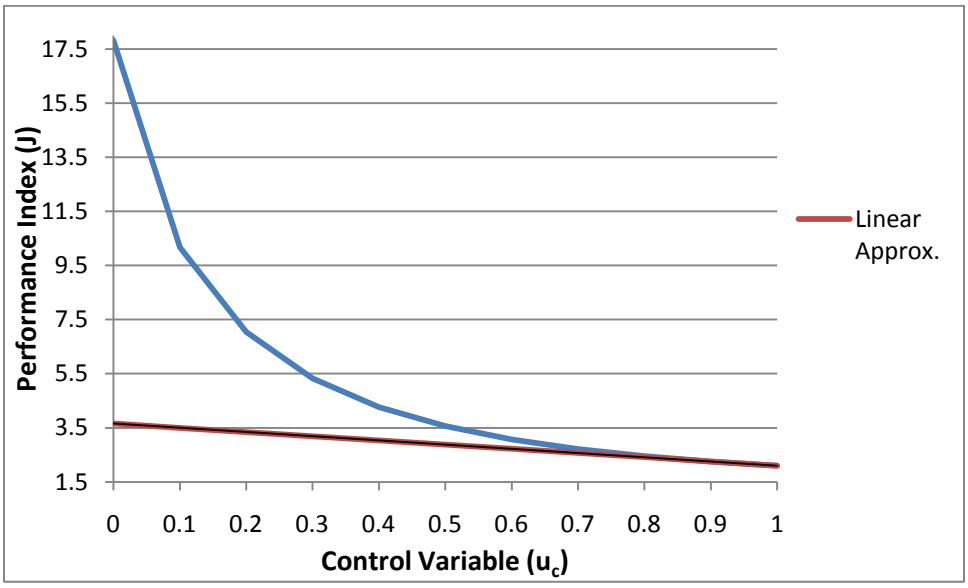

Figure 7.4. Results from circuit 3 outage for $J_{1,1}$.

Circuit 4 Outage

Figure 7.5 shows the results from the outage of circuit 4 and how well the linear approximation using $\Delta J = 0.229566$ is able to mimic the actual behavior of the PI shown in blue. This outage shows the PI dips slightly from the initial state of the system and then curves upwards more drastically as the control variable approaches zero, so that the overall change in the curve is positive. However, since the curve initially has a downward motion, the linear approximation has a positive slope, which is not the overall direction of this PI curve for this outage. This approximation looks poor, but the scale of

the difference between the PI curve and line is only approximately 0.5 out of a peak value of the PI curve of 2.4, so the estimation error of the outage (when $u_c = 0$) is around 20%.

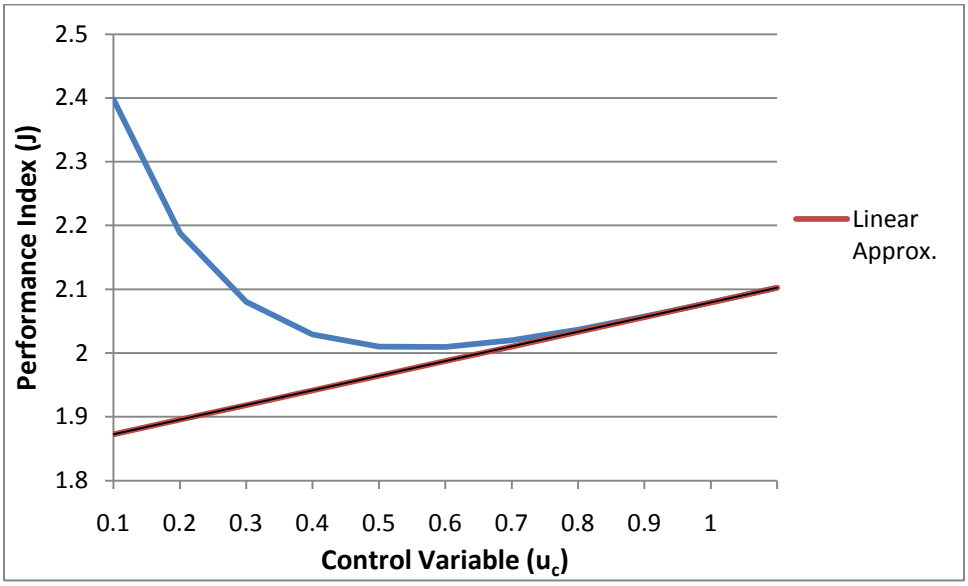

Figure 7.5. Results from circuit 4 outage for $J_{1,1}$.

Circuit 5 Outage

The results from the final circuit outage are shown in Figure 7.6 where the linear approximation uses a value of $\Delta J = 0.749702$ to approximate the blue line. The PI curve for this outage also slopes upward as the control variable approaches zero, but it initially dips down more than it slopes upward. Therefore the overall result is a negative change in the PI value, so a linear approximation using a positive slope is a fairly accurate representation of the behavior of the curve. Although the curves cross each other more than once, the PI curve's final outage value (when $u_c = 0$) is only 0.5 greater than that of the linear approximation, so the error is still less than 30%.

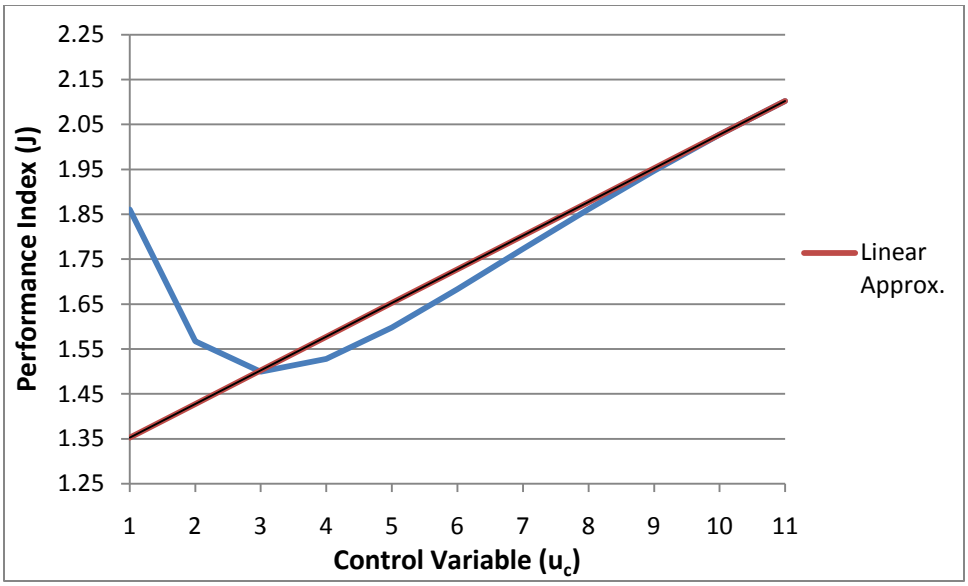

Figure 7.6. Results from circuit 5 outage for $J_{1,1}$.

Behavior of the Curves

The only common feature of all five PI curves is found in their behavior as the control variable approaches zero. As the outage approaches, the slopes all turn upwards, which is expected with an outage since the PI definition is the sum of the squares of each line's current loading compared to its rating. Therefore, with one line out of service, the remaining lines will be more heavily loaded, so the ratios of the remaining lines' loading to rating values will increase. The most drastic change in the PI curve and also the largest magnitude of a linear approximation's slope are found when circuit 2 is outaged. This outage affects the ratios of the loading to rating of the circuits in the system the most of all five lines tested because this line's rating is over twice that of the others, so it carries much more current than the other lines. Therefore it is a much heavier burden on the system when this line is out of service as compared to the other lines.

Performance Index $J_{1,2}$ ($\propto$=2)

The problem is formulated in a similar fashion as before, but for this index, the value of $\propto$ is double, so the PI becomes more nonlinear than the previous $J_{1,1}$. As described in Chapter 6, the change in the performance index (ΔJ) is approximated for each circuit outage. The data that simulates the performance index curves in Figures 7.7–7.11 is given in Table B.4, for the outages of circuits 1–5.

Circuit 1 Outage

The results from when circuit 1 is outaged are shown in Figure 7.7 where the blue line indicates the actual value of the PI, and the red line approximates this curve using $\Delta J = -0.12633$. This result is similar to the one shown in Figure 7.2, except the change in the PI curve is not as large and the slope has a greater magnitude but is still negative. The PI curve likewise has an upwards slope for all values of the control variable. The linear approximation deviates as the value of u_c drops below 0.7, but the difference between the line and PI curve is only 0.3 (when $u_c = 0$) on a scale where the peak value is 1.9, so the error is only 16%.

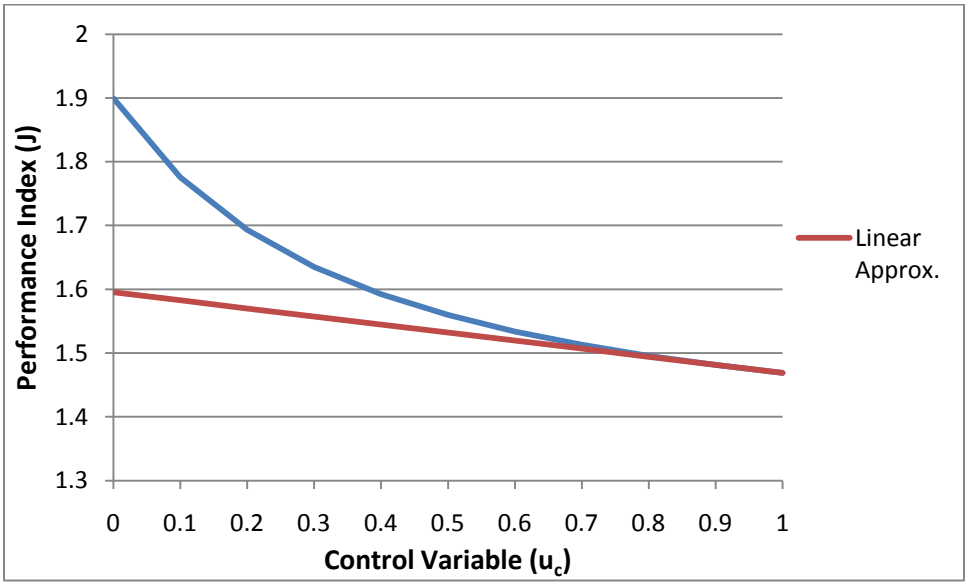

Figure 7.7. Results from circuit 1 outage for $J_{1,2}$.

Circuit 2 Outage

Figure 7.8 presents the results from when circuit 2 is outaged where the red line is the linear approximation of the blue curve with a slope value of $\Delta J = 0.38446$. The curve's shape mirrors that of the curve shown in Figure 7.3, except the values of the curve are different. The slope is still positive and of similar magnitude to the slope found for the $J_{1,1}$ index, except the slope for this outage is of slightly greater magnitude. It appears there is a large error between the linear approximation and PI curve when $u_c = 0$, but the scale of the figure is such that the value of the difference is only about 0.15 on a scale where the largest magnitude is around 1.25, so the error in estimating the outage is just over 16%.

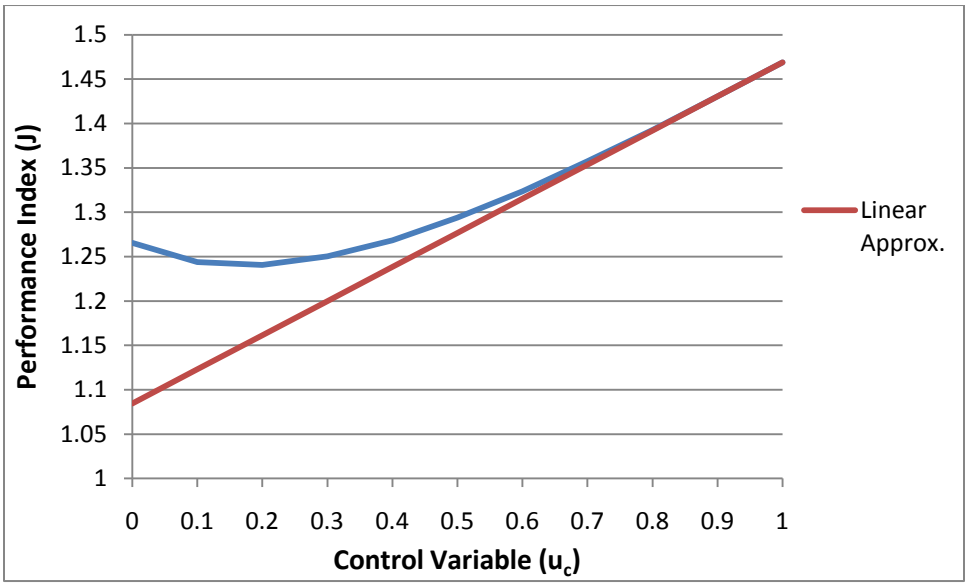

Figure 7.8. Results from circuit 2 outage for $J_{1,2}$.

Circuit 3 Outage

The results from the outage of circuit 3 are shown in Figure 7.9. The blue line shows the nonlinear PI curve, and the linear approximation is shown in the red line, which has a calculated slope of $\Delta J = -2.81688$. This PI curve shows a drastic change

from the initial state of the system and slopes upwards sharply just as this outage does for the index $J_{1,1}$ except the values are approximately ten times as great in Figure 7.9 as those in Figure 7.4. The line's slope is similarly negative, but the magnitude is greater for the $J_{1,2}$ index. The difference between the linear approximation and PI curve is much greater for this more nonlinear case than it was when $\propto = 1$, and the scale of the difference is an order of 10 larger than that shown in Figure 7.4. The error in the approximation of the circuit 3 outage is over 97% for this index.

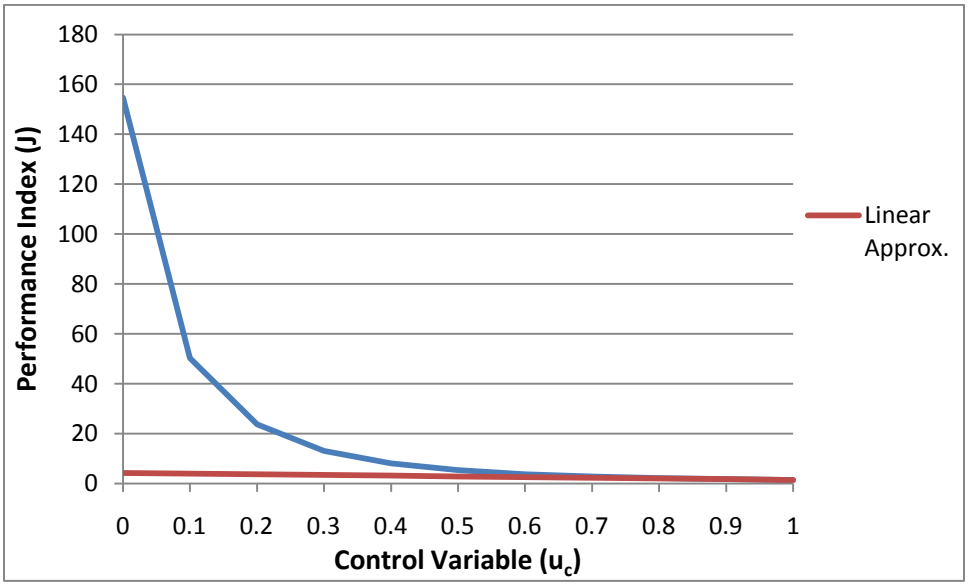

Figure 7.9. Results from circuit 3 outage for $J_{1,2}$.

Circuit 4 Outage

The outage of circuit 4 results in a PI curve as shown in blue in Figure 7.10, and the linear approximation uses a slope of $\Delta J = 0.498841$. The shape of this curve and of its linear approximation emulate the PI curve and line given in Figure 7.5, except the values are not as large for this index ($J_{1,2}$). The slope of the linear approximation in each case are both positive with the magnitude of the slope for this index being greater than it is for the previous index. The red line approximates the blue PI curve well until the value

of the control variable falls below 0.4, and it appears the two curves split quickly, leaving a large error for the outage (when $u_c = 0$). However, the actual difference between the curves is approximately 0.5 on a scale with the largest value at almost 1.5 on the PI curve, so the error of the outage estimation is just over 30% for this circuit's outage using the $J_{1,2}$ index.

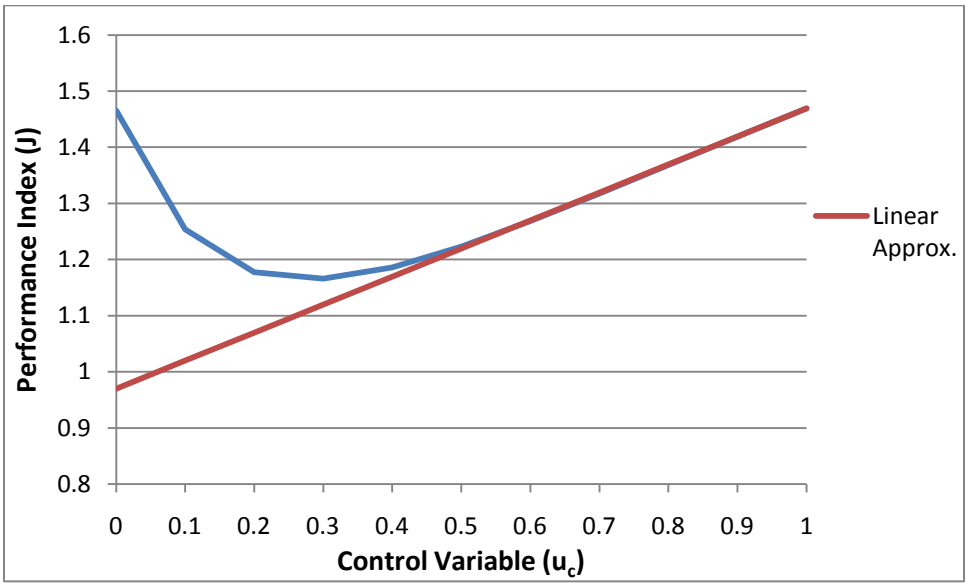

Figure 7.10. Results from circuit 4 outage for $J_{1,2}$.

Circuit 5 Outage

The results from the final circuit outage are shown in Figure 7.11, where the red line gives the linear approximation of the blue PI curve using $\Delta J = 1.26009$. The shape of this curve is similar to the curve shown in Figure 7.6, and the slope of the linear approximation is a larger positive value than the one for the previous index. However, the behavior of the PI curve for this index changes positively from the initial state of the system, while it has an overall negative change for the $J_{1,1}$ index. Therefore, a positive slope for this curve does not accurately depict the overall behavior of the PI when circuit 5 is outaged. Although this figure shows similar results when compared to the previous

PI and the error for the outage of this circuit for the $J_{1,1}$ index is under 30%, the scale for this case is much larger so the actual error is much greater for the $J_{1,2}$ index. The difference of the curves is approximately 2.0 on a scale where the highest value of the PI curve is 2.5 for the outage, so the error is very high and over 90% for the outage of circuit 5 using the $J_{1,2}$ index.

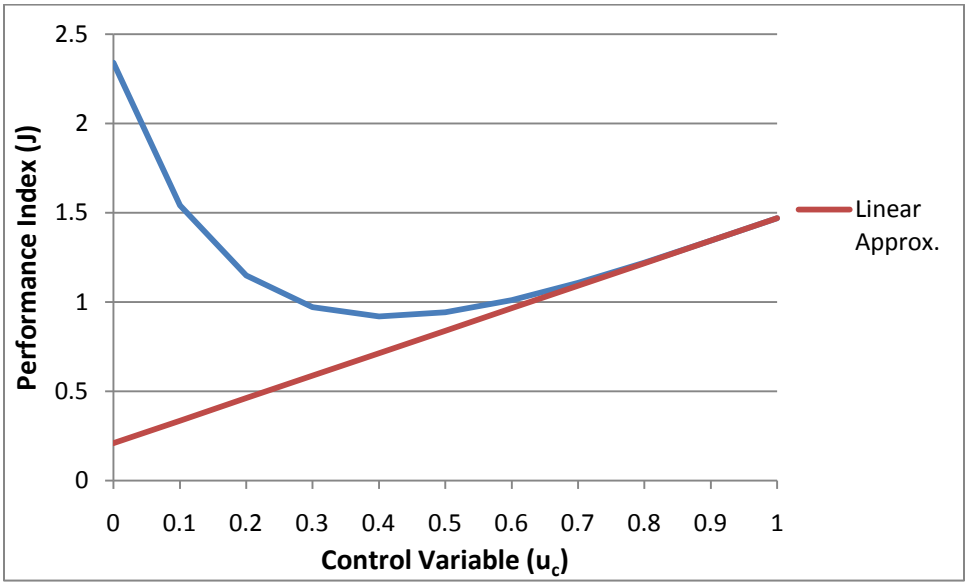

Figure 7.11. Results from circuit 5 outage for $J_{1,2}$.

Behavior of the Curves

The results shown in Figures 7.7–7.11 are similar to the ones given in the case when $\propto = 1$ for $J_{1,1}$ (Figures 7.2 –7.6) since both the shape of corresponding outage curves and the sign (positive or negative) of the slope values (ΔJ) for corresponding outages are the same. The magnitude of the slopes is greater for every outage using the definition of the $J_{1,2}$ index, and the values of the PI curves varied between being greater or smaller than those shown in the corresponding outages using the $J_{1,1}$ PI definition. The major change for the outages presented can be seen in the outage of circuit 5. The linear approximation gives a correct indication as to the behavior of the PI curve for $J_{1,1}$,

but when the definition of the index is more nonlinear ($J_{1,2}$), the linear approximation no longer indicates the overall change in the PI curve.

7.1.3 Proposed (More Linear) Performance Index J_2

The linear approximation of the performance index is shown in comparison to the true behavior of the performance index for single branch contingencies for this more linearized index definition. The outage is again simulated by allowing the control variable (u_c) to approach zero, and the difference between the linear approximation and PI curve at the time of the outage determines how well the given PI definition estimates each outage.

The problem for the index J_2 is formulated exactly as described in Chapter 6, and each single line contingency linear approximation is found using the process described. The linear approximation is compared to the estimated actual PI performance for each contingency to show how the two compare in each case. The data that simulates PI curves for the outages of circuits 1–5 is shown in Figures B.5–B.9, respectively.

Circuit 1 Outage

The result from the circuit 1 outage is shown in Figure 7.12 where the blue line shows the actual PI curve, and the red line gives the linear approximation using $\Delta J = -0.12599$. This shape is similar to the PI curves from both previous indices ($J_{1,1}$ and $J_{1,2}$) since it slopes upwards from the initial state of the system. The linear approximation has a negative slope, just like the other two presented for $J_{1,1}$ and $J_{1,2}$ (approximately -0.06 and -0.13, respectively), but this slope has a higher magnitude like the one found for the outage of circuit 1 using the index $J_{1,2}$. The difference between the blue and red lines at the time of the outage ($u_c = 0$) is around 0.15, which is approximately half the difference in the case of the $J_{1,1}$ index, and the scale is over twice as large since the

highest value for the PI curve is over 6.0, so the magnitude of the error is much smaller at around 2.5% compared to almost 7% for the $J_{1,1}$ index.

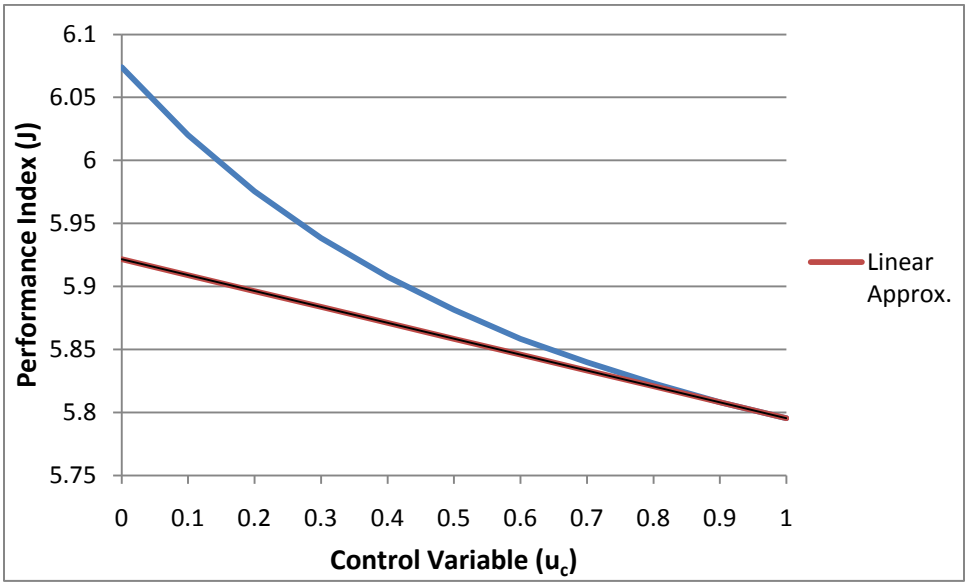

Figure 7.12. Results from circuit 1 outage for J_2.

Circuit 2 Outage

Figure 7.13 shows the results from the outage of circuit 2. The red line shows the linear approximation of the blue curve using a slope of $\Delta J = 0.31955$. The PI curve has a different curvature than the two seen for the previous indices $J_{1,1}$ and $J_{1,2}$ since it curves downward from the value of the initial state of the system. The linear approximation has a positive slope, however, which is similar to the results of the more nonlinear indices. The magnitude of the slope is between the previous two slopes since the approximation slopes for $J_{1,1}$ and $J_{1,2}$ are approximately 0.26 and 0.38, respectively, so the result from this index is also of similar magnitude. The value of the gap between the linear approximation and PI curve for the outage is nearly 3.0, which is much larger than it was for the nonlinear indices, but the scale for this index is almost three times the value of the scale for the previous indices, so the resulting error is only slightly higher at around 6%.

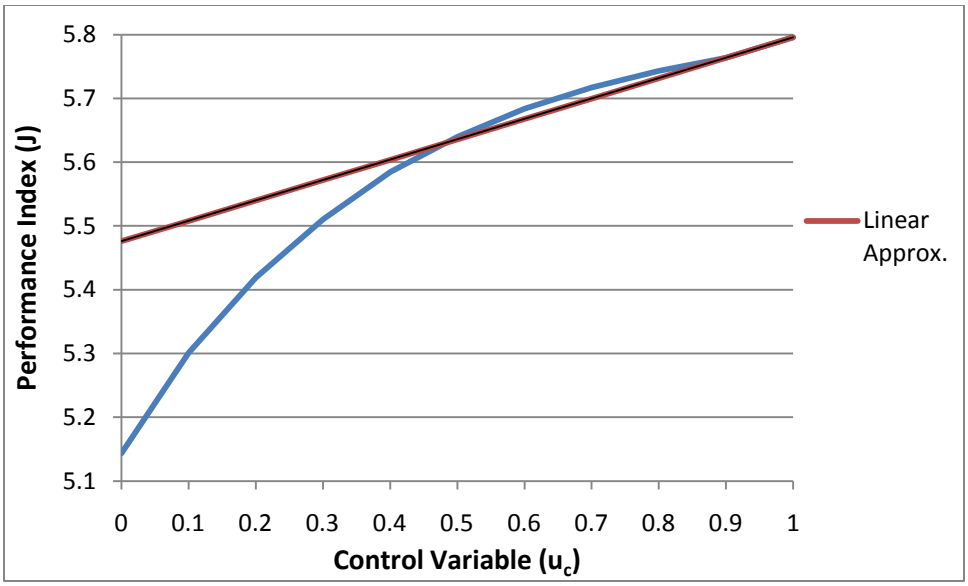

Figure 7.13. Results from circuit 2 outage for J_2.

Circuit 3 Outage

The outage of circuit 3 gives the results displayed in Figure 7.14, where the blue curve shows the actual PI value, and the red line approximates the curve using $\Delta J = -3.06383$. This PI curve has very similar shape and curvature as those found for the outage of circuit 3 for the more nonlinear indices $J_{1,1}$ and $J_{1,2}$, but the magnitude of the values of the curve more closely resemble those found for $J_{1,1}$. The slope for the linear approximation in this case is of similar magnitude to the slopes found for the other two indices (approximately -1.55 and -2.82, respectively), but the magnitude is slightly greater for this more linearized index. The scale for these results is similar to the one shown for the outage of this circuit using the $J_{1,1}$ index, but the slope of the line is more steep for this index, so the estimation error of the outage (when $u_c = 0$) is of smaller magnitude at just under 65% as opposed to just under 80% for the $J_{1,1}$ index.

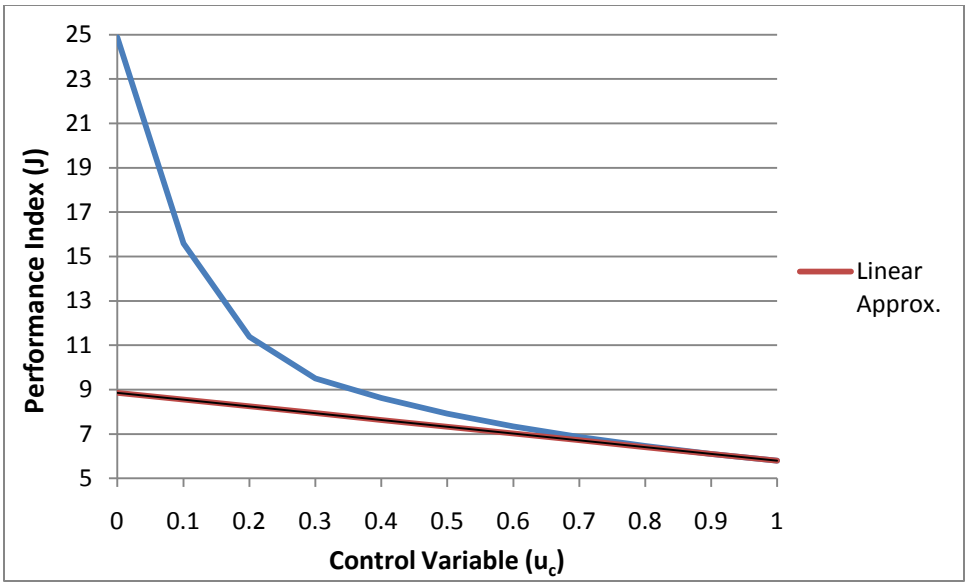

Figure 7.14. Results from circuit 3 outage for J_2.

Circuit 4 Outage

The results from the outage of circuit 4 are shown in Figure 7.15 where the red line approximate the blue PI curve using a slope of $\Delta J = 0.28495$. The curvature of the PI curve is downward for this index (J_2), where it instead points upwards for both the previous indices ($J_{1,1}$ and $J_{1,2}$). The slope of the linear approximation, however, is the same sign (positive) as those found for the previous two indices. The magnitude of the slope more closely resembles the approximation found for the index $J_{1,1}$ (approximately 0.23), but they are all of a relatively similar magnitude since the slope for the index $J_{1,2}$ is approximately only 0.5. Although the shape of the curves are vertically flipped compared to those shown in Figure 7.5, the shape is the same and the scale is of the same order of magnitude compared to the one for the $J_{1,1}$ index. The gap between the line and PI curve is nearly 1.0 for this index and approximately 0.5 for the $J_{1,1}$ index, but the scale for this index includes values over double that of the previous scale, so the resulting error is similar at around 23.5% compared to 22% for the $J_{1,1}$ index.

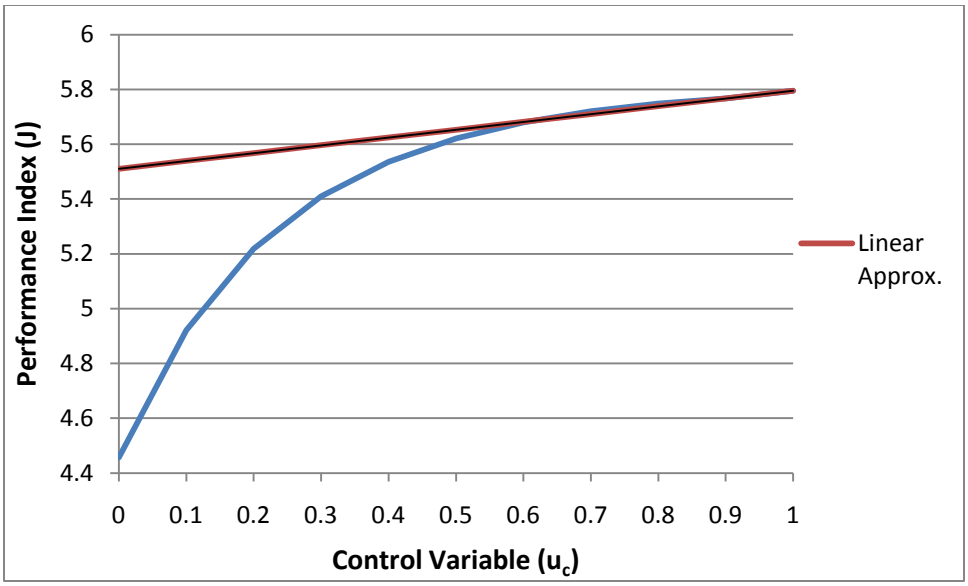

Figure 7.15. Results from circuit 4 outage for J_2.

Circuit 5 Outage

The results from the final outage of circuit 5 are given in Figure 7.16 such that the blue curve is the true PI value, and the red line gives the approximation, which has slope $\Delta J = 0.56793$. The shape of the PI curve resembles that of the PI curves for the indices $J_{1,1}$ and $J_{1,2}$, but it is not as smooth as those found for the other two indices. The slope of the linear approximation has the same sign (positive) as those found for the previous two indices, but it has a slightly smaller magnitude than the other two slopes (approximately 0.75 and 1.26, respectively). The shape of the curve resembles that of the one for the $J_{1,1}$ index, where the gap between the line and PI curve is nearly 2.0 for this index and around 0.5 for the $J_{1,1}$ index. Although the size of the gap is almost four times as large for this index (J_2), the scale is over three times that as the one seen for the $J_{1,1}$ index, so the outage estimation error is only slightly greater than that found for the $J_{1,1}$ index at just under 31% compared to 27%.

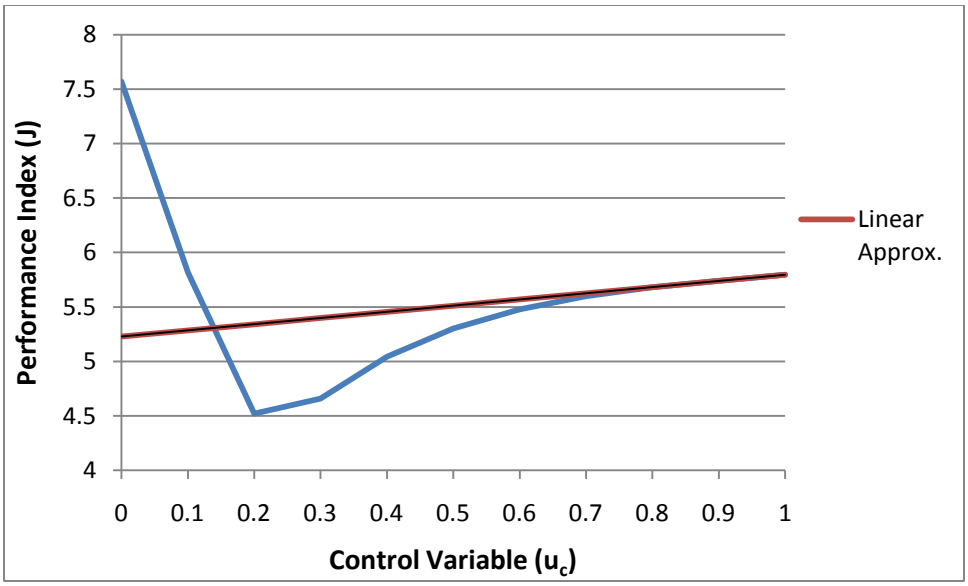

Figure 7.16. Results from circuit 5 outage for J_2.

Behavior of the Curves

Some of the curves for the J_2 index bear resemblance to the curves from the more nonlinear PI cases. Although the curves do not have the same curvature, all the slopes of the linear approximations (ΔJ) are similar since they have the same sign (positive or negative) and are of like magnitude for each corresponding contingency.

This index considers the difference between the overloads and margins of the lines in the system, where the overloads are defined as a result of the max function and margins as the min function as given in (7.3). The outages where the PI curvatures differ from the corresponding results of the more nonlinear indices include the outage of circuit 2 and circuit 4. Since the J_2 index uses the difference of the overloads and margins for each outage and since these PI curves point downwards instead of upwards, these outages result in reduced overloads along these two lines for each of their corresponding outages. When the line between buses 2 and 3 (circuit 4) of Figure 7.1 is in service, the system overloads this line trying to send the power to the load drop at bus 4. However, when it is out of service, this line cannot be overloaded so the overloads in the system are

reduced. Similarly, circuit 2 (between buses 1 and 3), is normally overloaded since it also is a main pathway to send generation to the load at bus 4, so when it is out of service, the overloads of the system are reduced. The extreme case in the system occurs with the loss of circuit 3 (between buses 1 and 4) since this line has a higher current rating than the others and is the only direct line between one of the two sources and the load drop at bus 4. In the case of this outage, the rest of the lines in the system would be overloaded, and this behavior is reflected in Figure 7.14 where it is clear that the overloads (i.e. positive values from the max function) increase as the control variable approaches zero.

7.2 Chapter Summary

The results from each circuit outage for three different performance indices are presented in this chapter. Two PI definitions are highly nonlinear, and their results are compared to those of the more linear, proposed PI definition. Section 7.1.2 presents the results of the first nonlinear index where the PI value slopes upward for each contingency as the control variable approaches zero (complete outage). The largest change results from the outage of circuit 3 because this circuit carries the largest load of any of the lines in the system. Section 7.1.3 shows the results from each circuit outage using the more nonlinear index's definition. The shapes of the PI curves are similar to those shown in Section 7.1.2, and the linear approximation values are of similar sign and magnitude for each corresponding contingency.

The results from the two nonlinear indices are then contrasted with those of the more linear, proposed index given in Section 7.1.4. The results from the proposed definition show the PI curves for the outages are similarly-shaped for most outages except for those with negative changes in the PI and positive linear approximation slopes from the nonlinear indices (circuit 2 and circuit 4 outages). The downward curvature of

these PI curves explains more about the behavior of the system without losing the accuracy of the sign of the linear approximation's slope since it remains similar to the previous two nonlinear indices. The figures from these three indices are presented in this chapter, but more details regarding the accuracy and utility of each of these indices are discussed in Chapter 8.

CHAPTER 8

CONCLUSIONS, CONTRIBUTIONS, AND RECOMMENDATIONS

8.1 Comparing Results

Although the shapes of the curves for each PI examined and the calculated slope (ΔJ) for corresponding contingencies are similar, the accuracies of the linear approximations produced by the different PI definitions show a pronounced difference. The percentage error for the highly nonlinear definitions ($J_{1,1}$ and $J_{1,2}$) are given in Table 8.1 and Table 8.2, respectively. The error increases significantly as the order increases since some of the errors shown in Table 8.2 (when $\propto = 2$) are more than double the size of the corresponding error when $\propto = 1$. The highest percent error for $J_{1,1}$ occurs when this corresponding circuit (circuit 3) is outaged. Circuit 3 has a line rating more than double that of the other lines in the network, so this result is reasonable since the biggest change would come with the largest loss, especially since this line is one of only two lines carrying power to the load at Bus 4. The error of the linear approximations of each single line contingency for the proposed (less nonlinear) method are given in Table 8.3. Though some of the values are negative, it is really the magnitude that needs to be compared. Some of the individual values have magnitudes slightly higher than those shown in $J_{1,1}$ (e.g. circuit 2), but the worst contingency in this system (circuit 3), has about 15% less relative error than the approximation using $J_{1,1}$.

Table 8.1. Linear Approximation Error Compared to PI Curve for $J_{1,1}$.

Circuit	Error (%)
1	6.879
2	5.527
3	79.485
4	21.915
5	27.306

Table 8.2. Linear Approximation Error Compared to PI Curve for $J_{1,2}$.

Circuit	Error (%)
1	16.008
2	16.674
3	97.228
4	33.780
5	91.072

Table 8.3. Linear Approximation Error Compared to PI Curve for J_2.

Circuit	Error (%)
1	-2.511
2	6.070
3	-64.394
4	23.652
5	-30.942

It is obvious that both $J_{1,1}$ and J_2 provide more accurate linear approximations of each respective PI than $J_{1,2}$. Although it may not be clear by looking at the errors of the individual contingencies, the average approximation error for the system gives a more clear indication of which PI introduces less error. Table 8.4 shows the average of the magnitudes of the approximation errors for each contingency for all three methods examined. As expected, the error for $J_{1,2}$ far exceeds the other two indices at over 50% average error. The proposed method (J_2), which is slightly less nonlinear than $J_{1,1}$,

introduces only 25.5% error, while $J_{1,1}$ introduces 28.2% error. The reduction in error between $J_{1,1}$ and J_2 is over 9.5%.

Table 8.4. Comparison of Average Errors for $J_{1,1}$, $J_{1,2}$, and J_2.

Method	Average Error (%)
Highly Nonlinear (α=1) ($J_{1,1}$)	28.222
Highly Nonlinear (α=2) ($J_{1,2}$)	50.952
Proposed Method (J_2)	25.514

The two highly nonlinear PI definitions $J_{1,1}$ and $J_{1,2}$ are both commonly used; however, they both introduce error in approximating the nonlinear PI curves that define the actual response of the system to a specific contingency. Since the average error of $J_{1,1}$ for the given test system is almost half that of $J_{1,2}$, $J_{1,1}$ is clearly the more accurate option for the current method of PI definitions. However, the proposed index definition (J_2) reduces the error from $J_{1,1}$ by over 9.5%. This decrease in error can be attributed to formulating the definition of the PI in a way that is slightly less nonlinear (ie more linear) than the previous definitions. Although both PI definitions of $J_{1,1}$ and J_2 compare the current loading of the line with its nominal rated value, the proposed, more linear PI J_2 provides a better approximation, which will result in more accurate contingency analysis results and fewer misrankings.

8.2 Contributions

The original and novel research performed in this work of developing a more accurate performance index compares the proposed linear index to other more nonlinear indices. This research presents the state equations using the QPF model, which increases efficiency of solving the system's equations since all equation models (shown in Chapter 4 and in more detail in Chapter 6) are of quadratic order. The proposed, more linear index is provided in detail in Chapter 6, and single line contingency results from a four

bus test system are presented and compared in Chapter 7. The curves in Chapter 7 show that this index can provide more detailed information about the behavior of the system while still maintaining the appropriate linear approximation direction. The accuracies given in Section 8.1 indicate that the proposed index also provides a more accurate approximation of the change in the behavior of the proposed index than the other, more nonlinear index approximations estimate their relative PI changes. The index definition, which is more linearized by using the QPF model, increases the ability of a linear approximation to estimate its PI curve, which is necessary for accurate contingency analysis.

8.3 Recommendations for Future Research

8.3.1 Other Applications and Expansion of Proposed Index's Use

This proposed, more linear performance index is defined on the basis of comparing the loading current of a line and the rated current. However, this definition is not limited to just the circuits in a system. A similar definition could be applied to other elements in the system such as bus voltages. The difference between the system's measured voltage and the nominal voltage could be used instead of the current values used in the given, proposed PI. Since this method is more linear than similar highly nonlinear methods currently in use, the results will be the same as those presented in this research – a reduction in the approximation error.

8.3.2 Further Linearization of Performance Index

Although the proposed performance index (J_2) is more linear than the ones to which it is compared, it could be made even more linear. Instead of using the difference of the squares of the current loading and rated values, the linear difference could be used. This PI, called J_3, is defined as shown in (8.1) where the y_{km} variables are defined in

(8.2) as the linear difference between the current loading and rated value. The same process for formulating the equations can be used as the one presented in Chapter 6, but the equations for $g_{x_{PI}}(x_{PI})$ will no longer have a quadratic structure due to the presence of a square root term introduced with representing I_{km} as opposed to ${I_{km}}^2$.

$$J_3 = \sum y_{km,over} - \sum y_{km,margin} \tag{8.1}$$

$$\begin{cases} y_{km,over} = max\{I_{km} - I_{km,0}, 0\} \\ y_{km,margin} = min\{I_{km} - I_{km,0}, 0\} \end{cases} \tag{8.2}$$

The results from this latest PI definition prove its utility nonetheless. The results from the same test system (Figure 7.1) are given in Figures 8.1–8.5 for the outages of circuits 1–5, respectively. There is less of a nonlinear behavior in the blue curves, which corresponds to the more linearized problem definition in (8.2). The data used to produce the blue PI curves is given in Tables B.10–B.14, respectively. The percentage error of the linearized approximation compared to the actual PI curve for each circuit outage is given in Table 8.5, with the error for circuit 3 having a smaller magnitude by over 10% than the proposed index J_2. The average error for the system with this definition is approximately 19.8%, which is an improvement over $J_{1,1}$ by almost 30% and over J_2 by over 22%. This PI definition in (8.1) and (8.2) still provides more accurate results and deserves to be investigated further, but it does not have the benefit of the higher efficiency since the quadratic structure of some of the equations is broken.

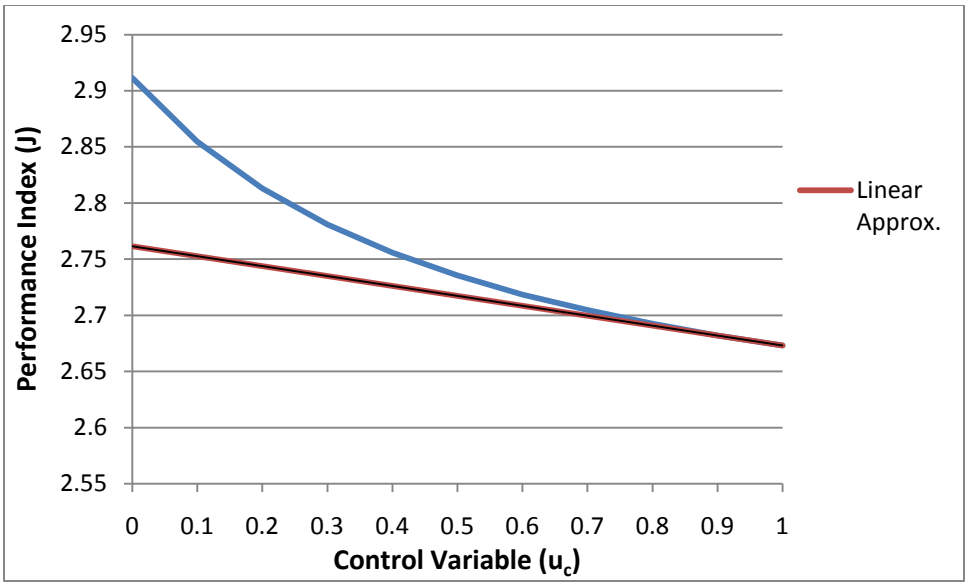

Figure 8.1. Results from circuit 1 outage for J_3.

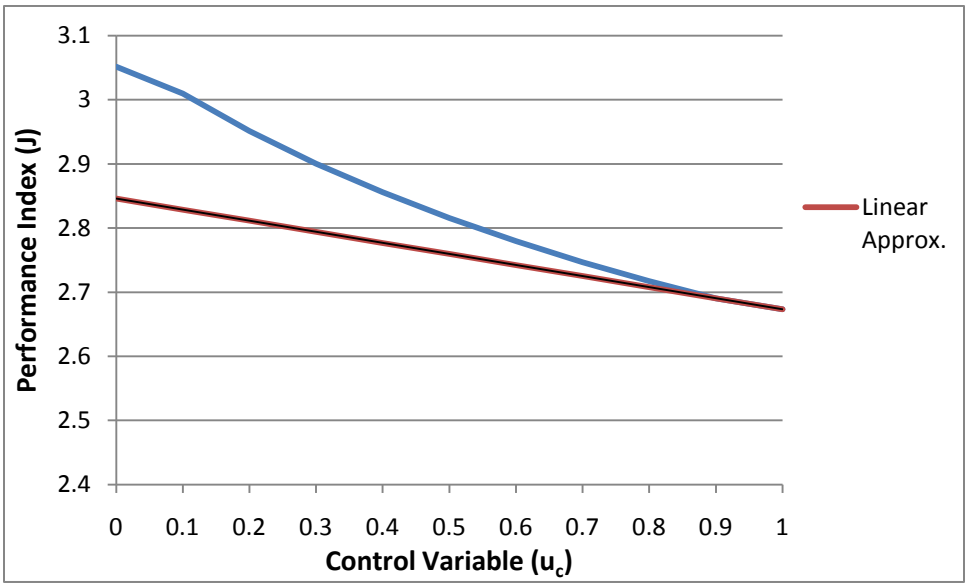

Figure 8.2. Results from circuit 2 outage for J_3.

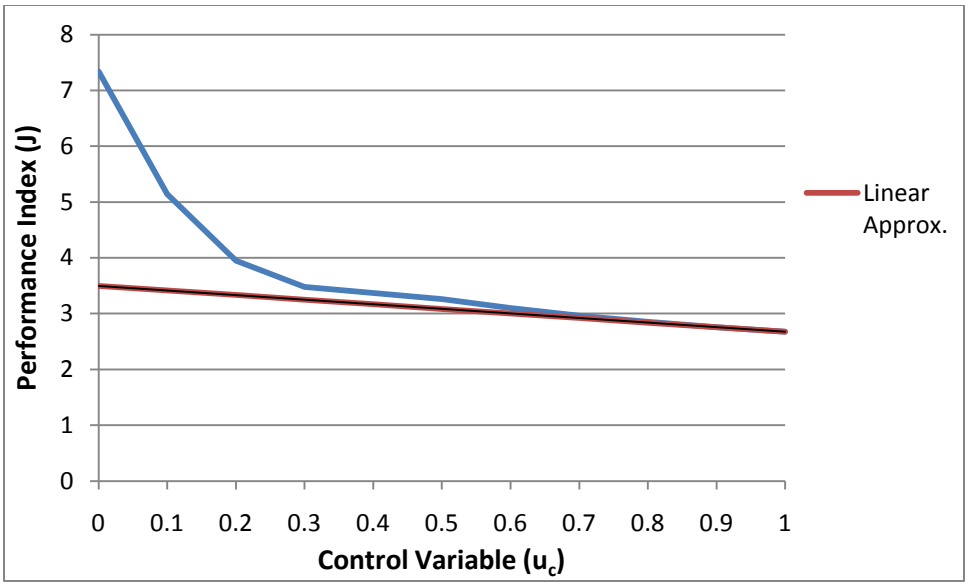

Figure 8.3. Results from circuit 3 outage for J_3.

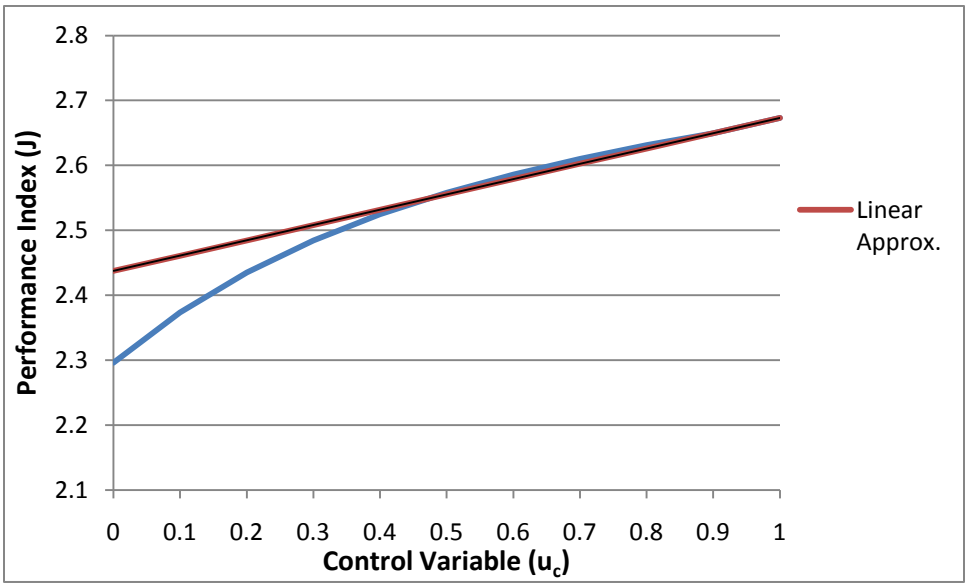

Figure 8.4. Results from circuit 4 outage for J_3.

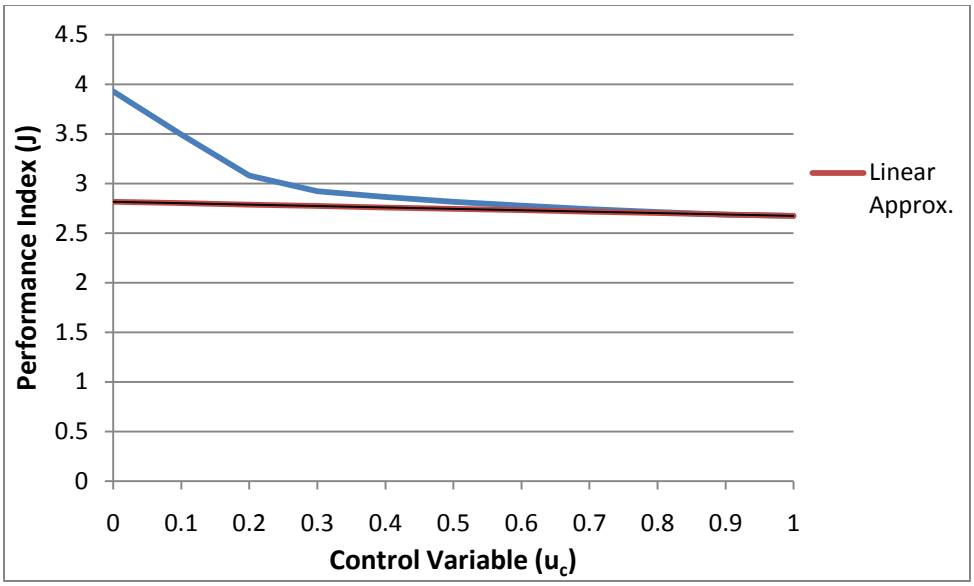

Figure 8.5. Results from circuit 5 outage for J_3.

Table 8.5. Linear Approximation Error Compared to PI Curve for J_3.

Circuit	Error (%)
1	-5.149
2	-7.218
3	-52.331
4	6.151
5	-28.368

APPENDIX A

SPARSITY TECHNIQUES

A.1 LU Factorization

Calculations of the solution to the common linear algebra problem, given in (A.1), can be simplified when dealing with a sparse matrix $\boldsymbol{A}$ to take advantage of the abundance of zero entries and increase efficiency of the calculations. The Sparsity software, *CSpatrix*, provided by Dr. George Cokkinides, uses LU Factorization method (or Gaussian Elimination) with Partial Pivoting to increase the speed of the computations [14]. Using LU Factorization method breaks the matrix *A* into lower and upper triangular matrices ($\boldsymbol{L}$ and $\boldsymbol{U}$, respectively), as shown in (A.2), which can be reorganized as the equations shown in (A.3) [15]. Introducing a new vector variable, $\boldsymbol{y}$, as shown in (A.4) allows the equation to be broken into two parts, shown in (A.5) [15]. Forward substitution is used to solve for the new variable $\boldsymbol{y}$ from the first equation since $\boldsymbol{L}$ is a lower triangular matrix, and back-substitution is then used to solve for the desired vector $\boldsymbol{\chi}$ [15].

$$\begin{cases} \boldsymbol{Ax} = \boldsymbol{b} \\ \boldsymbol{A} \in \mathbb{R}^{nxn}, \boldsymbol{x} \in \mathbb{R}^{nx1}, \boldsymbol{b} \in \mathbb{R}^{nx1} \end{cases} \tag{A.1}$$

$$\boldsymbol{A} = \boldsymbol{LU} \tag{A.2}$$

$$(\boldsymbol{LU})\boldsymbol{\chi} = \boldsymbol{b} \Leftrightarrow \boldsymbol{L}(\boldsymbol{U\chi}) = \boldsymbol{b} \tag{A.3}$$

$$\boldsymbol{y} = \boldsymbol{U\chi} \tag{A.4}$$

$$\begin{cases} \boldsymbol{Ly} = \boldsymbol{b} \\ \boldsymbol{U\chi} = \boldsymbol{y} \end{cases} \tag{A.5}$$

The *CSpatrix* software is especially efficient since it allocates memory storage only for those elements that are non-zero [14]. The matrix $\boldsymbol{A}$ is computed separately, and its terms are added to its Spatrix (sparse matrix counterpart) only if the value is above a given epsilon ($\in = 10^{-8}$). By considering only the non-zero terms, the *CSpatrix* matrix class further simplifies the number of calculations necessary to solve (A.1).

A.1.1 Application to the Contingency Analysis Process

The *CSpatrix* software was used any time an equation of the form given in (A.1) needed to be solved for a vector $\boldsymbol{\chi}$. There are two places in the code where problems of this form appear, and since power systems can generate a large number of equations, the matrix $\boldsymbol{A}$ can be very large, which makes finding $\boldsymbol{A^{-1}}$ impractical. The *CSpatrix* software was used in both the first and second steps of the process diagram shown in Figure 3.2. Both steps involve solving for the inverse of a Jacobian matrix. Since most buses in power systems do not have many lines tying them to the rest of the network, the power system can be called loosely connected. Additionally, since the Jacobian is formed based on the topology of the system, there will be many entries that will be blank (or, zero). It is this nature of the Jacobian that makes it a sparse matrix since it contains mostly zeros.

Solving the State of the System

The first step involves finding the solution of the state of the power system, which, as given in (3.4), requires finding the inverse of the Jacobian of the power equations $\left(\frac{\partial \boldsymbol{g}(\boldsymbol{x}_n)}{\partial \boldsymbol{x}}\right)$. This inverse must be found for each iteration in order to converge upon a final solution $\boldsymbol{x}_{n+1}$, thus, this matrix is converted to its Spatrix counterpart each iteration. Using the sparsity technique during this part of the process improves efficiency

of the process greatly since for each iteration, only approximately one-third of the steps necessary to find the inverse are needed to solve for the state of the system using sparsity techniques [15].

Solving for the Costate Vector

The second step in the process involves finding the costate vector $\widehat{\boldsymbol{x}}^{\boldsymbol{T}}$, which also involves finding the inverse of the Jacobian of the system $\left(\frac{\partial \boldsymbol{g}(\boldsymbol{x})}{\partial \boldsymbol{x}}\right)$ as seen in (3.5). However, this Jacobian has been augmented compared to the one used in the first step of the process, so finding its inverse would be even more time-consuming. Using the Spatrix counterpart of this matrix when solving for the costate vector also allows for large time savings and gained efficiency compared to finding the inverse of this matrix [15].

APPENDIX B

ADDITIONAL DATA

B.1 Introduction

The data used to generate the graph shown in Figure 1.1 in Chapter 1 came from the U.S. Energy Information Administration's total energy consumption by countries between 1980 and 2006 [1]. The data is given in Table B.1.

Table B.1. Total Energy Consumed in United States in 1980-2006 [1].

Year	Energy Consumed (10^9 kWh)
1980	2,094.45
1981	2,147.10
1982	2,086.44
1983	2,150.95
1984	2,285.80
1985	2,323.97
1986	2,368.75
1987	2,457.27
1988	2,578.06
1989	2,755.64
1990	2,837.08
1991	2,886.06
1992	2,897.21
1993	3,000.70
1994	3,080.89
1995	3,163.96
1996	3,253.77
1997	3,301.85
1998	3,425.10
1999	3,483.72
2000	3,592.36
2001	3,557.11
2002	3,631.65
2003	3,662.03
2004	3,715.95
2005	3,810.98
2006	3,816.85

B.2 Test System and Results

B.2.1 Test System Data (PTI Format)

The PTI format for the four-bus test system described in Chapter 7 is given in Table B.2 [12]. The file has been modified to make it easier to read, and lines have been introduced to divide the four sections of the file from which data is obtained for the analysis of this system. All data that is italicized in the file has been added to give the headings for each section and each column of data. The name of each section is given at the top: Case Identification, Bus Data, Generator Data, and Branch Data. The information used in each section is highlighted by the red text. In the Case Identification section, the system power base is given as 100 MVA ($SBASE$). In the Bus Data section, the data from the columns labeled I, IDE, PL, QL, GL, BL, VM, and VA are used, which correspond to the bus number, bus type, real power of constant power load at the bus, reactive power of constant power load at the bus, shunt conductance of constant power load at the bus, shunt susceptance of constant power load at the bus, bus voltage magnitude, and bus voltage angle, respectively. In the Generator Data section, the data from the columns labeled I, ID, PG, QG, VS, $IREG$, $MBASE$, ZR, ZX, and $STAT$ are used, which correspond to the bus number to which the generator is connected, the generator's mode of operation identifier, real power generated, reactive power generated, bus voltage setpoint, operation mode of generator, total power base of the generator, the internal resistance, and the internal reactance, respectively. Finally, from the Branch Data section, data from the columns labeled $Bus\ k$, $Bus\ m$, CKT, R, X, B, $RATEA$, and ST are used where these variables refer to the bus number on the sending end of a line, bus number on the receiving end of a line, circuit number, line resistance, line reactance, shunt terms of the line, MVA power rating of the line, and the status of the line. The zeros at the bottom of the Data sections indicate the end of the data in that section.

Table B.2. PTI Format for Test System Input Data.

Case Identification

0 100.00 / FRI MAR 06 2009 00:00

05/22/09 GT POWER 100.0 1979 S

Bus Data

I	*IDE*	*PL*	*QL*	*GL*	*BL*	*IA*	*VM*	*VA*	*NAME*	*BASKV*	*ZONE*
1	3	0	0	0	0	1	1	0	Bus1	115	1
2	2	0	0	0	0	1	1	0	Bus2	115	1
3	1	0	0	0	0	1	1	0	Bus3	115	1
4	1	280	50	0	0	1	1	0	Bus4	115	1
0											

Generator Data

I	*ID*	*PG*	*QG*	*QT*	*QB*	*VS*	*IREG*	*MBASE*	*ZR*	*ZX*	*RT*	*XT*	*GTAP*	*STAT*	*RMPCT*	*PT*	*PB*
1	0	0	0	0	0	0	0	0	0	1	0	0	1	1	0	0	0
2	1	80	0	0	0	1	0	0	0	1	0	0	1	1	0	0	0
0																	

Branch Data

Bus k	*Bus m*	*CKT*	*R*	*X*	*B*	*RATEA*	*RATEB*	*RATEC*	*RATIO*	*ANGLE*	*GI*	*BI*	*GJ*	*BJ*	*ST*
1	2	1	0	0.1	0	110	125	130	0	0	0	0	0	0	1
1	3	1	0	0.125	0	110	125	130	0	0	0	0	0	0	1
1	4	1	0	0.08	0	250	270	280	0	0	0	0	0	0	1
2	3	1	0	0.11111	0	110	125	130	0	0	0	0	0	0	1
3	4	1	0	0.08333	0	110	125	130	0	0	0	0	0	0	1
0															

B.2.2 Performance Index Curve Approximations

The data for the resulting PI curves given in Figures 7.2–7.6 is shown in Table B.3. Also, the data for the resulting plots given in Figures 7.7–7.11 is shown in Table B.4. These results were obtained using a power systems analysis simulation software called WinIGS to approximate the outage of each circuit for the various control variable parameter's values (one through zero) to simulate the circuit both in service and out of service.

The data for the PI curve approximation used in Figures 7.12–7.16 are given in Tables B.5–B.9, respectively. The data that corresponds to the PI curves shown in Figures 8.1–8.5 is provided in Tables B.10–B.14, respectively. These results are also obtained using WinIGS simulations and varying the circuit parameters to simulate the outage of each line.

Data for $J_{1,1}$

Table B.3. Results from Circuit 1-5 Outages for $J_{1,1}$.

u_c	Circuit 1	Circuit 2	Circuit 3	Circuit 4	Circuit 5
0	2.324	1.943	17.814	2.398	1.860
0.1	2.258	1.930	10.160	2.188	1.567
0.2	2.215	1.930	7.041	2.080	1.500
0.3	2.185	1.941	5.325	2.029	1.528
0.4	2.163	1.956	4.266	2.010	1.598
0.5	2.147	1.977	3.563	2.010	1.683
0.6	2.134	1.999	3.074	2.020	1.773
0.7	2.123	2.025	2.720	2.037	1.862
0.8	2.115	2.050	2.457	2.057	1.947
0.9	2.108	2.076	2.257	2.079	2.027
1	2.102	2.102	2.102	2.102	2.102

Data for $J_{1,2}$

Table B.4. Results from Circuit 1-5 Outages for $J_{1,2}$.

u_c	Circuit 1	Circuit 2	Circuit 3	Circuit 4	Circuit 5
0	1.899	1.265	154.639	1.465	2.339
0.1	1.775	1.244	50.218	1.253	1.541
0.2	1.693	1.241	23.715	1.177	1.149
0.3	1.635	1.250	13.136	1.166	0.970
0.4	1.592	1.268	8.067	1.186	0.919
0.5	1.560	1.294	5.341	1.223	0.941
0.6	1.534	1.323	3.759	1.268	1.010
0.7	1.513	1.357	2.788	1.318	1.107
0.8	1.495	1.393	2.165	1.368	1.221
0.9	1.482	1.430	1.751	1.419	1.343
1	1.469	1.469	1.469	1.469	1.469

Data for J_2

Table B.5. Results from Circuit 1 Outage for J_2.

u_c	Overload	Margin	Overload – Margin
0	0.176	-5.898	6.074
0.1	0.134	-5.886	6.020
0.2	0.104	-5.871	5.975
0.3	0.082	-5.857	5.938
0.4	0.064	-5.843	5.908
0.5	0.050	-5.831	5.881
0.6	0.039	-5.820	5.859
0.7	0.029	-5.811	5.840
0.8	0.021	-5.802	5.823
0.9	0.014	-5.794	5.808
1	0.008	-5.787	5.796

Table B.6. Results from Circuit 2 Outage for J_2.

u_c	Overload	Margin	Overload – Margin
0	0.000	-5.144	5.144
0.1	0.000	-5.301	5.301
0.2	0.000	-5.419	5.419
0.3	0.000	-5.510	5.510
0.4	0.000	-5.585	5.585
0.5	0.000	-5.640	5.640
0.6	0.000	-5.684	5.684
0.7	0.000	-5.717	5.717
0.8	0.000	-5.743	5.743
0.9	0.000	-5.764	5.764
1	0.008	-5.787	5.796

Table B.7. Results from Circuit 3 Outage for J_2.

u_c	Overload	Margin	Overload – Margin
0	17.673	-7.208	24.882
0.1	8.504	-7.080	15.584
0.2	4.704	-6.676	11.380
0.3	2.918	-6.582	9.500
0.4	2.014	-6.607	8.621
0.5	1.396	-6.523	7.919
0.6	0.953	-6.392	7.345
0.7	0.622	-6.242	6.864
0.8	0.368	-6.087	6.455
0.9	0.168	-5.934	6.102
1	0.008	-5.787	5.796

Table B.8. Results from Circuit 4 Outage for J_2.

u_c	Overload	Margin	Overload – Margin
0	0.000	-4.457	4.457
0.1	0.000	-4.922	4.922
0.2	0.000	-5.218	5.218
0.3	0.000	-5.410	5.410
0.4	0.000	-5.536	5.536
0.5	0.000	-5.621	5.621
0.6	0.000	-5.680	5.680
0.7	0.000	-5.720	5.720
0.8	0.000	-5.749	5.749
0.9	0.000	-5.767	5.767
1	0.008	-5.787	5.796

Table B.9. Results from Circuit 5 Outage for J_2.

u_c	Overload	Margin	Overload – Margin
0	3.159	-4.411	7.570
0.1	1.394	-4.423	5.817
0.2	0.240	-4.282	4.522
0.3	0.000	-4.658	4.658
0.4	0.000	-5.042	5.042
0.5	0.000	-5.301	5.301
0.6	0.000	-5.478	5.478
0.7	0.000	-5.600	5.600
0.8	0.000	-5.680	5.680
0.9	0.000	-5.739	5.739
1	0.008	-5.787	5.796

Data for J_3

Table B.10. Results from Circuit 1 Outage for J_3.

u_c	Overload	Margin	Overload – Margin
0	0.077	-1.100	2.912
0.1	0.059	-1.058	2.855
0.2	0.047	-1.028	2.813
0.3	0.037	-1.004	2.781
0.4	0.029	-0.986	2.756
0.5	0.023	-0.971	2.735
0.6	0.017	-0.959	2.718
0.7	0.013	-0.949	2.705
0.8	0.009	-0.940	2.693
0.9	0.006	-0.933	2.682
1	0.004	-0.927	2.673

Table B.11. Results from Circuit 2 Outage for J_3.

u_c	Overload	Margin	Overload – Margin
0	0.000	-3.051	3.051
0.1	0.000	-3.009	3.009
0.2	0.000	-2.951	2.951
0.3	0.000	-2.900	2.900
0.4	0.000	-2.856	2.856
0.5	0.000	-2.816	2.816
0.6	0.000	-2.780	2.780
0.7	0.000	-2.747	2.747
0.8	0.000	-2.717	2.717
0.9	0.000	-2.690	2.690
1	0.004	-2.669	2.673

Table B.12. Results from Circuit 3 Outage for J_3.

u_c	Overload	Margin	Overload – Margin
0	4.240	-3.098	7.338
0.1	2.390	-2.751	5.140
0.2	1.415	-2.534	3.949
0.3	0.932	-2.549	3.481
0.4	0.696	-2.672	3.368
0.5	0.514	-2.744	3.259
0.6	0.371	-2.727	3.097
0.7	0.253	-2.711	2.964
0.8	0.156	-2.696	2.852
0.9	0.074	-2.682	2.756
1	0.004	-2.669	2.673

Table B.13. Results from Circuit 4 Outage for J_3.

u_c	Overload	Margin	Overload – Margin
0	0.000	-2.296	2.296
0.1	0.000	-2.373	2.373
0.2	0.000	-2.435	2.435
0.3	0.000	-2.484	2.484
0.4	0.000	-2.524	2.524
0.5	0.000	-2.558	2.558
0.6	0.000	-2.586	2.586
0.7	0.000	-2.610	2.610
0.8	0.000	-2.631	2.631
0.9	0.000	-2.650	2.650
1	0.004	-2.669	2.673

Table B.14. Results from Circuit 5 Outage for J_3.

u_c	Overload	Margin	Overload – Margin
0	0.567	-3.362	3.929
0.1	0.265	-3.228	3.493
0.2	0.048	-3.031	3.079
0.3	0.000	-2.921	2.921
0.4	0.000	-2.862	2.862
0.5	0.000	-2.814	2.814
0.6	0.000	-2.774	2.774
0.7	0.000	-2.741	2.741
0.8	0.000	-2.712	2.712
0.9	0.000	-2.687	2.687
1	0.004	-2.669	2.673

REFERENCES

[1] U.S. Energy Information Administration, “International Energy Annual 2006,” 8 December 2008, 13 January 2010, http:// www.eia.doe.gov/emeu/international/electricityconsumption.html.

[2] North American Electric Reliability Coordination, “Version Two Facilities Design, Connections and Maintenance Reliability’s Standards,” 6 July 2009, 26 February 2010, http://www.nerc.com/files/Final_Final_CompFiling-FAC_VRF_WECC.pdf.

[3] Chen, Y.; Bose, A.; , "An adaptive pre-filter for the voltage contingency selection function," *Power Industry Computer Application Conference, 1989. PICA '89, Conference Papers* , vol., no., pp.225-231, 1-5 May 1989.

[4] Stefopoulos, G.K.; Fang Yang; Cokkinides, G.J.; Meliopoulos, A.P.S.; , "Advanced contingency selection methodology," *Power Symposium, 2005. Proceedings of the 37th Annual North American* , vol., no., pp. 67- 73, 23-25 Oct. 2005.

[5] Zhenyu Huang; Yousu Chen; Nieplocha, J.; , "Massive contingency analysis with high performance computing," *Power & Energy Society General Meeting, 2009. PES '09. IEEE* , vol., no., pp.1-8, 26-30 July 2009.

[6] Yuan-Yih Hsu; Han-Ching Kuo; , "Fuzzy-set based contingency ranking [power system security]," *Power Systems, IEEE Transactions on* , vol.7, no.3, pp.1189-1196, Aug 1992.

[7] Bacher, R.; , "Graphical interaction and visualization for the analysis and interpretation of contingency analysis results," *Power Industry Computer Application Conference, 1995. Conference Proceedings., 1995 IEEE* , vol., no., pp.128-134, 7-12 May 1995.

[8] Musirin, I.; Rahman, T.K.A.; , "On-line voltage stability based contingency ranking using fast voltage stability index (FVSI)," *Transmission and Distribution Conference and Exhibition 2002: Asia Pacific. IEEE/PES* , vol.2, no., pp. 1118-1123 vol.2, 6-10 Oct. 2002.

[9] Musirin, I.; Khawa, T.; Rahman, A.; , "Simulation technique for voltage collapse prediction and contingency ranking in power system," *Research and Development, 2002. SCOReD 2002. Student Conference on* , vol., no., pp. 188- 191, 2002.

[10] Meliopoulos, A. P. Sakis, Class Notes: *Power System Monitoring, Analysis and Control*, Georgia Institute of Technology, ECE 6320: Power Systems Control and Operation, Fall 2008.

[11] Northeast Power Coordinating Council, Inc., "Procedure to Collect Power System Event Data for Analysis of System Performance," 25 September 2007, 26 February 2010, http://www.npcc.org/viewDoc.aspx?name=c-25.pdf&cat=regStandProced.

[12] "PTI Power Flow Data Format," University of Washington College of Engineering, January 2009, http://www.ee.washington.edu/research/pstca/formats/pti.txt.

[13] Meliopoulos, A. P. Sakis, Class Notes: *Comparison of Two Contingency Ranking Algorithms*, Georgia Institute of Technology, ECE 8901: Special Problems, Fall 2008.

[14] Cokkinides, George, (personal communication via email, george.cokkinides@ece.gatech.edu), CSpatrix C++ Class, October 30, 2009.

[15] Trefethen, Lloyd and David Bau, Numerical Linear Algebra, Philadelphia: Society for Industrial and Applied Mathematics (Siam), 1997, ISBN: 0-89871-361-7.